AN ANALYSIS OF THE LASER-DOPPLER VELOCIMETER AND ITS APPLICATION TO THE MEASUREMENT OF TURBULENCE

by

William Kenneth George, Jr.

A Dissertation Submitted to the Johns Hopkins University
in Conformity with the Requirements for the
Degree of Doctor of Philosophy

Baltimore, Maryland

1971

*AN ANALYSIS OF THE LASER DOPPLER VELOCIMETER AND ITS APPLICATION TO THE MEASUREMENT OF TURBULENCE**

by

William K. George, Jr.

Report to Fluid Mechanics Branch
U.S. Office of Naval Research
Department of the Navy
Under Contract N00014-67-A-0385-0013
with
Department of Aerospace Engineering
The Pennsylvania State University
University Park

September 1971

*Submitted in partial fulfillment of the requirements for the degree of Doctor of Philosophy in the Department of Mechanics of the Johns Hopkins University, May 1971

ABSTRACT

In 1964, Yeh and Cummins demonstrated that coherent light sources could be used for the measurement of steady fluid velocities by observing the Doppler shift in the frequency of light scattered from small particles moving with the fluid. Since 1964 many investigators have attempted to extend this technique to the measurement of turbulent velocity fluctuations.

A fundamental limitation on this type of velocimeter is the Doppler ambiguity introduced by the finite transit time of particles through the scattering volume, turbulent velocity fluctuations across the scattering volume, velocity gradients, aperture, and electronic noise. A unified account of the effect of the Doppler ambiguity is presented and results are interpreted using the power spectrum. The influence of the ambiguity on the measurement of other statistical quantities is also examined.

Limitations on the spatial and temporal resolution imposed by the finite sampling volume are examined using the power spectrum and criteria for optimization of the response are proposed.

An operational Laser-Doppler Velocimeter is described and measurements of spectra in both laminar and turbulent flow are presented. The experimental results are seen to be in excellent agreement with theoretical predictions.

ACKNOWLEDGEMENTS

The author wishes to express his sincere gratitude to Professor J. L. Lumley of the Pennsylvania State University for the opportunity to carry out this work under his direction at P.S.U. and his guidance and encouragement throughout the course of this investigation. The author is also grateful to Professor W. H. Schwarz of the Johns Hopkins University who coordinated many of the details of the author's graduate program.

In addition, the author would like to thank Professor H. Tennekes of the Pennsylvania State University for his timely advice and constructive criticism on many occasions and Professor S. Corrsin of the Johns Hopkins University for his encouragement and counsel throughout the author's studies.

The services rendered by Mr. R. Carlson and Mr. T. Gatski, who assisted with the experimental work, Mr. E. Jordan and Mr. R. Pierce, who built and maintained the electronics, and Miss Kathy Jones who assisted with the computer work contributed to make this investigation possible.

This list would be incomplete without an expression of appreciation to my wife, Mary Ann, and family for their support and encouragement.

This research was carried out at the Pennsylvania State University and supported in part by the Office of Naval Research, Department of the Navy under Contract Numbers Nonr 656(33) and N00014-67-A-0385-0013 and in part by the Ordnance Research Laboratory under contract with the Naval Ordnance Systems Command.

TABLE OF CONTENTS

TABLE OF ILLUSTRATIONS

LIST OF SYMBOLS

C_p	scattering constant defined in equation (2.12)
$dN(\alpha)$	fluctuating Fourier amplitude of $d\phi/dt$
$dZ(\alpha)$	fluctuating Fourier amplitude of ω_o
$d\xi(x_o)$	random variable accounting for the presence of the scatterers
$E(k)$	three-dimensional spectrum function of the turbulence
F_{11}	one-dimensional velocity spectrum defined by equation (3.6)
$\tilde{F}_{11}$	F_{11} non-dimensionalized by ε,ν
F_o	measured one-dimensional velocity spectrum defined by equation (3.7)
$\tilde{F}_o$	F_o non-dimensionalized by ε,ν
F,G	fluctuating amplitudes of the cosine and sine components of the Doppler signal
F',G'	values of F,G at time t'

f,g	fluctuating amplitudes of the cosine and sine components of the noise
f',g'	values of f,g at time t'
i	complex a.c. current defined by equation (2.6)
i_{s_p}	a.c. current generated by a single scattering particle
I	from equation (2.16), the amplitude of the current generated by a particle at the center of the scattering volume $NC_pU_iU_r$
I_o	modified Bessed function of the second kind
$\underset{\sim}{k}$	(k_1,k_2,k_3), the wavenumber vector of spatial variations in velocity
$\tilde{\underset{\sim}{k}}$	$\underset{\sim}{k}$ non-dimensionalized by η
$\tilde{k}_o$	dimensionless wavenumber at which the turbulence spectrum and ambiguity spectrum are equal
k_*	defined by equation (3.5)
$\tilde{k}_*$	k_* non-dimensionalized by η
$\tilde{k}_{*_{crit}}$	$\tilde{k}_*$ of minimum ambiguity defined by equation (7.1)

m_*	defined by equation (3.5)
$\tilde{m}_*$	m_* non-dimensionalized by η
$\tilde{m}_{*crit}$	$\tilde{m}_*$ of minimum ambiguity
n_*	defined by equation (3.5)
$\tilde{n}_*$	η_* non-dimensionalized by η
N	Chapter 2: defined by equation (2.3) Chapter 6 and Appendix 2: $N = \Delta\omega_f/\Delta\omega$
R	defined by (4.29)
R_1	$R/(\sin \theta/2)^{1/3}$
R_m	Reynolds number of flow based on grid mesh
t	time
$\underset{\sim}{u}$	(u,v,w), the velocity of the fluid
$\underset{\sim}{u}'$	(u',v',w'), the fluctuating fluid velocity
u_o	defined by equation (3.2), the weighted volume averaged velocity
u_o'	fluctuating part of u_o

$\bar{U}$ mean flow velocity

u_i amplitude of the scattering beam

U_i amplitude of the scattering beam at the center of focus

u_r amplitude of the reference beam

U_r amplitude of the reference beam at the center of focus

u_{s_i} amplitude of light scattered from the i^{th} particle

$\underset{\sim}{x}$ (x,y,z), the position coordinate defined using the flow

$\underset{\sim}{x}'$ (x',y',z), the position coordinate defined using the scattering beam (Figure 1)

$\underset{\sim}{x}''$ (x'',y'',z), the position coordinate defined using the reference beam (Figure 1)

$\underset{\sim}{x}_p$ (x_p,y_p,z_p), the position of scattering particle in the flow coordinates

$\underset{\sim}{x}_{p_o}, \underset{\sim}{x}_o$ initial position of scattering particle

y_d'' position of the photocell in the $\underset{\sim}{x}''$ - coordinate system

α	frequency
α_o	frequency at which turbulence spectrum and ambiguity spectrum are equal
β	Chapter 3:defined by equation (3.10) as sin $\Theta/2$ Chapter 4 and Appendices: $\beta = \sigma_\Delta \sigma_N$, the signal to noise ratio
γ	phase of signal from a single scatterer defined by equation (2.20)
Δu	difference between local velocity u and the weighted volume averaged velocity u_o
$\Delta\omega$	total Doppler bandwidth defined by equation (4.13)
$\Delta\omega_f$	half width of bandpass filter
$\Delta\omega_L$	bandwidth of the Doppler broadening due to the finite transit time of particles through the scattering volume
$\Delta\omega_T$	bandwidth of the Doppler broadening due to turbulent velocity fluctuations within the scattering volume
ϵ	rate of dissipation of turbulent energy
η	Kolmogorov microscale $(\nu^3/\epsilon)^{1/4}$
$\eta(\alpha)$	spectrum of the random phase fluctuations due to the Doppler ambiguity

η_D spectrum of the phase fluctuations due to the Doppler signal alone

η_N spectrum of the phase fluctuations due to the noise alone

η_I spectrum of the phase fluctuations due to the interaction between the noise and the Doppler signal

θ scattering angle

Θ fluctuating phase of the Doppler signal

κ wavenumber of light

λ wavelength of light

ν kinematic viscosity

ρ defined by equation (4.10)

ρ_D defined by equation (A2.7)

ρ_N defined by equation (A2.10)

σ Chapter 2,3: standard deviation of the reference and scattered beams at focus
Appendix 2: shorthand for σ_T

$\sigma_1, \sigma_2, \sigma_3$	defined by equation (3.3)
σ_D	root mean square Doppler signal
σ_N	root mean square noise
σ_T	root mean total signal
τ	time lag $(t'-t)$
Φ_{11}	(k_1, k_2, k_3), the spectrum of the u' - component of velocity
ϕ	phase angle of the Doppler signal defined by equation (4.9)
$\dot{\phi}$	$d\phi/dt$
$\dot{\phi}'$	$\dot{\phi}$ evaluated at time t'
ω'	Doppler frequency of a single particle defined by equation (2.19)
ω_o	Doppler frequency averaged over all particles in the volume
ω	difference frequency between ω' and ω_o

1 INTRODUCTION

1.1 General Statement of the Problem

The problem to be discussed here is whether a Laser-Doppler Velocimeter can be used in the measurement of turbulence; and if so, what are its limitations?

1.2 Relevance of the Problem

Because of the difficulties that have been encountered in the use of conventional heat transfer probes in certain non-Newtonian and high polymer flows (e.g. - Fabula (1966)), efforts have been made to develop alternate methods. One such method that has been suggested is the use of a Laser-Doppler Velocimeter. This instrument uses the Doppler shift of light scattered from moving particles in the flow to extract velocity information. The prime advantage of the Laser-Doppler Velocimeter is that it requires no obstructing devices to be placed in the flow which might influence the phenomenon being measured. A disadvantage is that a

scattering agent (usually in the form of suspended particles) must be present in the flow; in liquids, however, this generally is not a problem. If the Laser-Doppler Velocimeter could be shown to be a reliable and practical means of measuring turbulence, it would provide an attractive alternative to conventional techniques in many flow situations.

1.3 *Historical Background*

In 1964, Yeh and Cummins successfully measured velocity profiles in a liquid by examining the frequency shift in monochromatic radiation scattered from particles in the liquid. The scattered and unscattered radiation was heterodyned on a photocell producing an electrical signal at the difference frequency; the spectrum of this difference frequency was examined by conventional techniques. Since 1964, numerous investigators have applied this technique to the measurement of mean square fluctuating velocities and instantaneous velocities in the unsteady flow of gases and liquids (Foreman et. al. (1966), Pike et. al. (1968), Welch et. al.

(1968), and Lumley et. al. (1969)). Recent attempts have been made to measure turbulence in the atmosphere and ocean using radar and sonar as incident radiation (Wiseman (1969), Little (1965), Thermitte (1968)).

1.4 Nature of the Problem

Considerable attention has been given in the literature to the choice of optical components, scattering particles, and electronic signal processing (Huffaker et. al. (1969), Mayo (1969), Davis (1968), Rolfe et. al. (1968)). The sources of noise have been identified and theory for optimization of the signal-to-noise ratio has been developed. In spite of these advances, the most basic question has not been answered; that is, how does the instantaneous Doppler frequency relate to the instantaneous flow velocity?

The fundamental problem in attempting to relate the Doppler frequency and the flow velocity is that even in a steady laminar flow the Doppler frequency is not steady. The signal received by the photocell is the sum of the

signals produced by all the scatterers present in the scattering volume at that instant; the individual signals may have the same frequency, but each has a phase dependent on its position in the scattering volume at some arbitrarily chosen origin in time as well as an intensity dependent on the particle size. As scatterers leave the scattering volume and new ones enter, the signal gradually loses coherence; when the entire population has changed, all coherence is lost. Velocity gradients, turbulent velocity fluctuations in the scattering volume, receiver aperture, and electronic noise arising from the detection process may also contribute to a loss of coherence.

1.5 *The Scope of This Investigation*

This paper will first examine the spatial and temporal resolution of the Laser-Doppler Velocimeter and criteria for meaningful measurement will be established. Second, the effect of the random phase fluctuations introduced by the Doppler ambiguity on attempts to measure statistical

quantities in turbulent flow will be examined. An exact theory for the statistics of the phase fluctuations will be presented. Third, an operational Laser-Doppler Velocimeter will be described and measurements in both laminar and turbulent flow will be presented.

2 SPATIAL AND TEMPORAL DEPENDENCE OF THE PHOTOELECTRIC CURRENT

2.1 Spatial Dependence of the Photoelectric Current*

The typical Laser-Doppler Velocimeter employs a scattering beam which is focused at some region in the flow and which is scattered from neutrally buoyant particles suspended in the flow. This scattered radiation is collected by a photocell and mixed with a reference beam which has not been scattered.

If $\hat{u}_r(x'',y_d'',z,t)$ and $\hat{u}_{s_i}(x'',y_d'',z,t)$ represent respectively the reference beam and light scattered from the i^{th} particle in the coordinate system defined by the photocell (see Figure 1) we may write

$$\hat{u}_r(x'',y_d'',z,t) = u_r(x'',y_d'',z)e^{j2\pi ft} \qquad (2.1)$$

*The analysis of this section follows closely that of Mayo (1969).

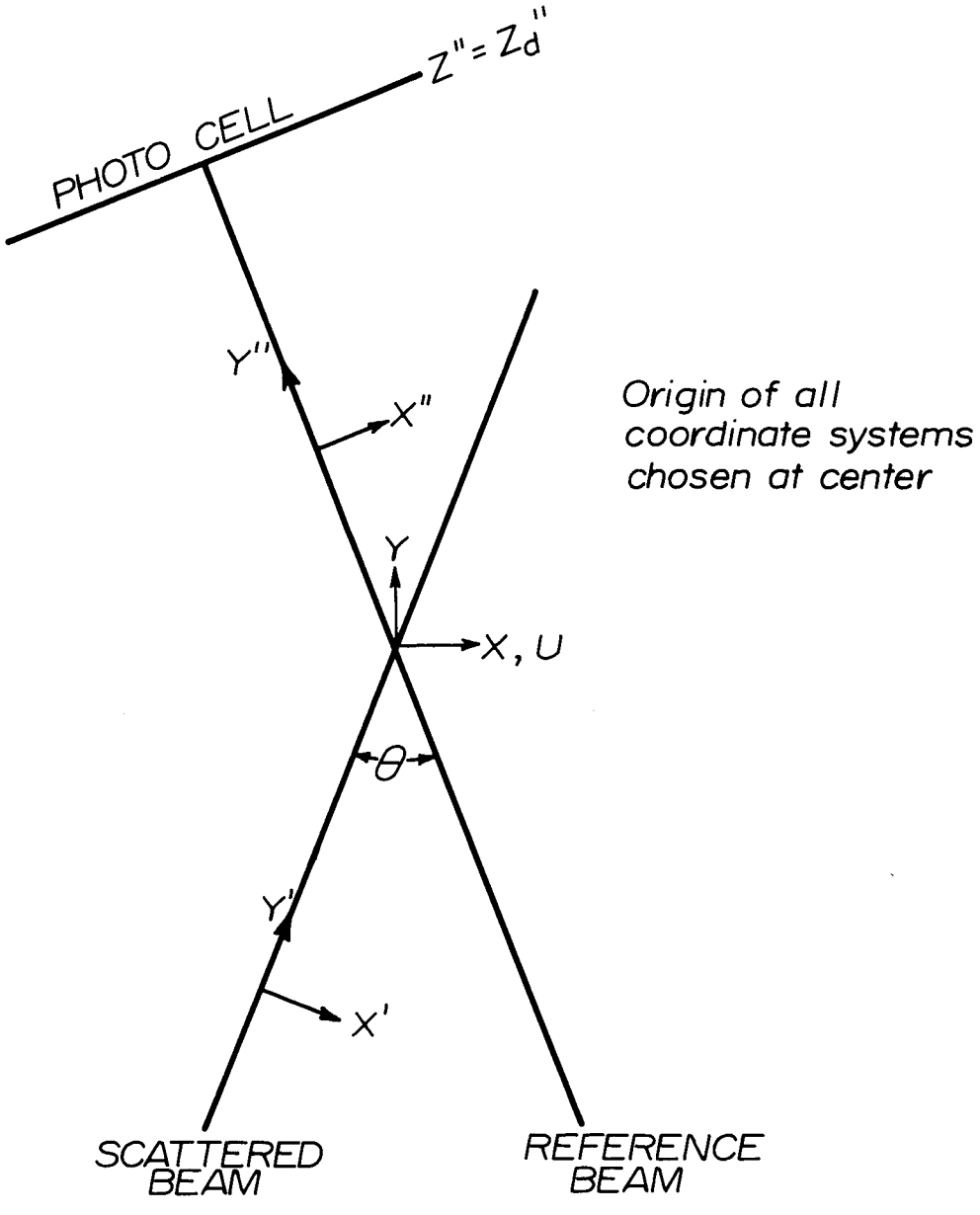

Figure 1: Scattering Coordinates with Origins Chosen at Center of Scattering Volume.

$$\hat{u}_{s_i}(x'',y_d'',z,t) = u_{s_i}(x'',y_d'',z)e^{j2\pi ft} \qquad (2.2)$$

where u_r and u_{s_i} are the respective complex amplitudes and where f is the frequency of the unscattered radiation. For simplicity the source of light has been assumed monochromatic.

The current at the photocell is then given by the integral over the photosensitive surface of the intensity of the light striking it; hence

$$i_{total} = N \iint_S \left| u_r(x'',y_d'',z) + \sum_i u_{s_i}(x'',y_d'',z) \right|^2 dx''dz \qquad (2.3)$$

where

S = photosensitive surface

N = $\delta e/hf$

δ = quantum efficiency of photocell

e = electronic charge

h = Planck's constant

and where the summation is over all contributing scattering particles. Expanding the integrand of (2.3) we have

$$i_{total} = N \iint_S \{u_r u_r^* + u_r \sum_i u_{s_i}^* + u_r^* \sum_i u_{s_i} + \sum_i \sum_j u_{s_i} u_{s_j}^* \} dx'' dz \tag{2.4}$$

We may immediately identify the integral of the first term as the direct current produced by the reference beam alone; that is,

$$i_{d.c.} = N \iint_S u_r u_r^* dx'' dz \tag{2.5}$$

Since u_r is usually much larger than the u_{s_i}, it is this term that is primarily responsible for the photon shot noise at the photocell (see Ross (1967)).

It will be shown later that the frequency of moving particles is Doppler shifted; hence, the last integral of (2.4) will contribute only in the frequency range from zero to a value representative of the maximum velocity *differences* in the volume, and in a similar symmetric interval around *twice* the mean Doppler frequency. If we are narrow band filtering we will *not* see this.

For convenience we will define i as the complex alternating current where

$$i = N \iint_S u_r^* \sum_i u_{s_i} \, dx'' dz \tag{2.6}$$

Clearly $i_{a.c.}(t)$ real is given by

$$i_{a.c.}(t) = i + i^* \tag{2.7}$$

If we change the order of summation and integration in (2.6) we have

$$i = N \sum_i \iint_S u_r^* u_{s_i} \, dx'' dz \qquad (2.8)$$

Thus the net time dependent current i is simply the sum of the currents generated by the individual scattering particles i_{s_p} where

$$i_{s_p} = N \iint_S u_r^*(x'', y_d'', z) \, u_{s_p}(x'', y_d'', z) \, dx'' dz \qquad (2.9)$$

u_{s_p}, the amplitude of the light scattered from the particle, may be approximated by the paraxial propagation of a spherical wave originating at the particle; that is,

$$u_{s_p}(x'',y_d'',z,t) = u_i(x_p',y_p',z_p')$$

(2.10)

$$\cdot (C_p/j\lambda(y_d''-y_p''))e^{j\kappa(y_d''-y_p'')+j\{\kappa[(x''-x_p'')^2+(z''-z_p'')^2]/2(y_d''-y_p'')\}}$$

where

$C_p = (j\lambda/2)\sqrt{\sigma_p^2/\pi}\ e^{j\phi}$

σ_p = the scattering cross-section of the particle

ϕ_p = relative phase of incident to scattered radiation

κ = wave number of light

p = denotes position of the particle

and $u_i(x_p',y_p',z_p')$ is the amplitude of the scattering beam at the particle position.

From equation (2.9) we have using (2.10)

$$i_{s_p} = N\, u_i(x_p', y_p', z_p)\, C_p\{[e^{jk(y_d''-y_p'')}/j\lambda(y_d''-y_p'')] \cdot \iint_S u_r^*(x'', y_d'', z) e^{jk[(x''-x_p'')^2 + (z-z_p)^2]/2(y_d''-y_p'')}\, dx''dz\} \tag{2.11}$$

The term in brackets has been identified by Mayo (1970) as the inverse propagation convolution of $u_r(x'', y_d'', z)$ and therefore specifies the form of the reference beam at the position of the particle; that is $u_r(x_p'', y_p'', z)$. Thus

$$i_{s_p} = N\, C_p\, u_i(x_p', y_p', z_p)\, u_r^*(x_p'', y_p'', z_p) \tag{2.12}$$

where it should be noted that u_i and u_r are expressed in different coordinate systems. A justification of (2.12) is provided in Appendix (1). It is important to note that (2.12) is true only if there are no spatial filters between the scattering volume and the photocell and if all apertures block

negligible reference beam intensity. These limitations have been discussed more fully by Mayo (1970).

We will determine u_i and u_r by focusing the Gaussian cross-section reference and scattered beams to their diffraction limited spot sizes at the desired flow location, hence

$$u_r(x'',y'',z) = U_r\, e^{-(x''^2 + z^2)/2\sigma^2}\, e^{j\kappa y''} \tag{2.13}$$

$$u_i(x',y',z) = U_i\, e^{-(x'^2 + z^2)/2\sigma^2}\, e^{j\kappa y'} \tag{2.14}$$

where σ is determined by

$$\sigma = \sqrt{2}\, f_o \lambda/\pi d \tag{2.15}$$

f_o is the focal length of the lens and d is the distance between the $1/e^2$ intensity points of the beam at the lens. For convenience we have chosen the focal length of the two

lenses to be equal; this is not necessary, although interpretation of results to be presented in following chapters becomes more difficult if different lenses are used. The depth of field of the lens has been ignored since for all reasonable focal length lenses it is much larger than the effective beam cross-section as defined by equation (2.16); hence the beam is considered constant along the direction of propagation.

Substitution of (2.13) and (2.14) into (2.12) and transformation to the flow coordinate system yields

$$i_{s_p}(t)=NC_pU_iU_re^{-(x_p^2\cos^2(\theta/2)+y_p^2\sin^2(\theta/2)+z_p^2)/\sigma^2} \cdot \cos[2\kappa x_p\sin(\theta/2)] \tag{2.16}$$

where (x_p,y_p,z_p) are the coordinates of the scattering particle.

2.2 *The Signal from Moving Particles*

We define $(x_{p_o}, y_{p_o}, z_{p_o})$ to be the initial position of the scattering particle which at time t is at (x_p, y_p, z_p) and require that u >> v,w; then, if the time for a particle to traverse the scattering volume (say $2\sigma/u$) is less than the smallest time scale of the turbulence (say $(\nu/\varepsilon)^{1/2}$), we may write

$$\begin{aligned} x_p &\simeq ut + x_{p_o} \\ y_p &\simeq y_{p_o} \\ z_p &\simeq z_{p_o} \end{aligned} \tag{2.17}$$

where the u for a particular particle is effectively constant as it moves through the volume. Then i_{s_p} is given by

$$i_{s_p}(t) = NC_p U_i U_r e^{-\{(x_{p_o}+ut)^2 \cos^2(\theta/2) + y_{p_o}^2 \sin^2(\theta/2) + z_{p_o}^2\}/\sigma^2} \cdot \cos(\omega' t + \gamma) \tag{2.18}$$

where the Doppler shift ω' is defined by

$$\omega' = 2\pi(2u/\lambda) \sin \theta/2 = 2\kappa u \sin \theta/2 \qquad (2.19)$$

and the phase γ is fixed by the initial x-coordinate of the particle

$$\gamma = 2\kappa x_{p_o} \sin \theta/2 \qquad (2.20)$$

For steady laminar flow in the x-direction the above expressions are exact. For turbulent flow the assumptions leading to (2.17) amount to Taylor's hypothesis (c.f. Lumley (1964)); namely, that the flow is effectively frozen in time as it is swept through the volume.

3 SPATIAL AND TEMPORAL RESOLUTION OF THE LASER-DOPPLER VELOCIMETER

3.1 The Effective Instantaneous Velocity

Before the Laser-Doppler Velocimeter can be used to provide reliable measurements in turbulent flow, its spatial and temporal resolution must be well understood. The frequency fluctuations arising from the Doppler scattering result only from the velocity component parallel to the difference wave number of the incident and scattered radiation; that is,

$$\omega' = (\underset{\sim}{\kappa}_i - \underset{\sim}{\kappa}_s) \cdot \underset{\sim}{u} \qquad (3.1)$$

where $\underset{\sim}{\kappa}_i$ and $\underset{\sim}{\kappa}_s$ are the wave number vectors of the incident and scattered light respectively. For the choice of coordinates in Figure (1), it is clear from equation (2.19) that the frequency fluctuations depend only on the u-velocity component.

The effective velocity seen by the velocimeter, say $u_o(t)$, is the average of the velocities of all the particles in the scattering volume - an average that is, of course, weighted by

the relative strength of the signal from each particle. Using the amplitude envelope for a single particle (determined in equation (2.16)) to characterize the scattering volume and normalizing the weighting to unity over the entire volume, it is easy to show that the effective velocity seen by the velocimeter is given by

$$u_o(t) = \int_{-\infty}^{\infty}\int\int u(x,y,z,t) \cdot \{1/(2\pi)^{3/2}\}e^{-\{(x^2/2\sigma_1^2) + (y^2/2\sigma_2^2) + (z^2/2\sigma_3^2)\}} \, dxdydz \tag{3.2}$$

where we have defined

$$\begin{aligned} \sigma_1 &= \sigma/\sqrt{2} \cos \theta/2 \\ \sigma_2 &= \sigma/\sqrt{2} \sin \theta/2 \\ \sigma_3 &= \sigma/\sqrt{2} \end{aligned} \tag{3.3}$$

$\sigma_1, \sigma_2, \sigma_3$ clearly measure the extent of the scattering volume in the x,y,z directions respectively.

3.2 *The Measured Velocity Spectrum*

By taking the Fourier transform of equation (3.2), it is not difficult to show, under the assumption that the turbulence is frozen as it moves through the volume, that the mean square velocity fluctuation $\overline{u_o'(t)^2}$ measured by the velocimeter is given by

$$\overline{u_o'(t)^2} = \overline{[u_o(t) - \overline{u_o(t)}]^2} \tag{3.4}$$

$$= \int_{-\infty}^{\infty}\int\int \Phi_{11}(k_1,k_2,k_3) e^{-\{(k_1^2/2\kappa_*^2)+(k_2^2/2m_*^2)+(k_3^2/2n_*^2)\}} dk_1 dk_2 dk_3$$

where $\Phi_{11}(k_1,k_2,k_3)$ is the velocity spectrum associated with the u- component of velocity, (k_1,k_2,k_3) are the wave number components of spatial variations of velocity in the (x,y,z) directions respectively, and (k_*,m_*,n_*) are cutoff wave numbers defined from the scattering volume dimensions as

$$\begin{aligned} k_* &= 1/\sqrt{2}\,\sigma_1 \\ m_* &= 1/\sqrt{2}\,\sigma_2 \\ n_* &= 1/\sqrt{2}\,\sigma_3 \end{aligned} \tag{3.5}$$

It is clear that contributions to (3.4) from spatial variations in velocity smaller than the extent of the scattering volume will be attenuated.

The one-dimensional velocity spectrum of the turbulence is defined by (c.f. Lumley (1964))

$$\overline{u'^2} = \int_{-\infty}^{\infty} F_{11}(k_1)\,dk_1$$

$$F_{11}(k_1) = \int\int_{-\infty}^{\infty} \Phi_{11}(k_1,k_2,k_3)\,dk_2\,dk_3 \qquad (3.6)$$

Using (3.4) the one-dimensional velocity spectrum measured by the Laser-Doppler Velocimeter, say $F_o(k_1)$, is seen to be defined by

$$\overline{u_o'^2} = \int_{-\infty}^{\infty} F_o(k_1)\,dk_1$$

$$F_o(k_1) = e^{-k_1^2/2k_*^2} \int\int_{-\infty}^{\infty} \Phi_{11}(k_1,k_2,k_3)\, e^{-\{(k_2^2/2m_*^2)+(k_3^2/2n_*^2)\}}\,dk_2\,dk_3 \qquad (3.7)$$

The relation between $F_o(k)$, the measured spectrum, and $F_{11}(k)$ the true spectrum is of course, of great interest.

If we restrict ourselves to isotropic turbulence we may write (c.f. Batchelor (1960))

$$\Phi_{11}(k_1,k_2,k_3) = (E(k)/4\pi k^4)[k^2-k_1^2] \tag{3.8}$$

where $k^2 = k_1^2 + k_2^2 + k_3^2$ and where $E(k)$ is the three-dimensional spectrum function (c.f. Batchelor (1960)). Using (3.8) it is not difficult to show that

$$F_{11}(k_1) = \tfrac{1}{2} \int_{k_1}^{\infty} (E(k)/k)[1 - (k_1^2/k^2)]dk \tag{3.9}$$

If we define

$$\beta = \sin \theta/2 \tag{3.10}$$

so that $m_* = \beta n_*$ from (3.5) and (3.3) and use (3.7), (3.8) it is more difficult, but straight-forward to show that

$$F_o(k_1) = e^{-k_1^2/2k_*^2} \tfrac{1}{2} \int_{k_1}^{\infty} (E(k)/k)[1 - (k_1^2/k^2)]$$

$$\cdot e^{-(k^2-k_1^2)(1+\beta^2)/4m_*^2} I_o\{(k^2-k_1^2)(1-\beta^2)/4m_*^2\}dk \qquad (3.11)$$

where I_o is the zeroth-order modified Bessel function of the second kind. Usually $\beta = \sin \theta/2$ is small since the scattering angle is small.

Pao's form of the spectrum E(k) is given by* (Pao (1966))

$$E(k) = \alpha k^{-5/3} \exp\{-(3/2)\alpha(k\eta)^{4/3}\} \qquad (3.12)$$

By substituting (3.12) into (3.11) and letting $\xi = k_1/k$ we have a form suitable for numerical computation

$$F_o(k_1) = e^{-k_1^2/2k_*^2} \alpha k_1^{-5/3} (1/2) \int_0^1 (1-\xi^2)\xi^{2/3} \exp\{-(3/2)\alpha(k_1\eta/\xi)^{4/3}\}$$

$$\cdot e^{-[k_1^2(1-\xi^2)(1+\beta^2)/4m_*^2\xi^2]} I_o[k_1^2(1-\xi^2)(1-\beta^2)/4m_*^2\xi^2]d\xi \qquad (3.13)$$

*η is the Kolmogorov microscale defined by $\eta = (\nu^3/\varepsilon)^{1/4}$ where ε is the rate of dissipation and ν is the kinematic viscosity.

It is convenient to nondimensionalize by Kolmogorov variables ε, ν where ν is the kinematic viscosity and ε is the rate of dissipation of turbulent energy; we have

$$k_1 \eta = \tilde{k}_1 \qquad m_* \eta = \tilde{m}_*$$

$$(1/\varepsilon^{1/4} \nu^{5/4}) F(k_1) = \tilde{F}(\tilde{k}_1)$$

$\tilde{F}_o(\tilde{k}_1)$ has been computed from (3.13) and is shown in Figure (2) for several values of $\tilde{m}_*$ where $\beta = 0.145$. The true spectrum $\tilde{F}_{11}(\tilde{k}_1)$ is also shown for comparison. It is clear that when $\tilde{k}_1$ becomes of order $\tilde{m}_*$, the spectrum shows significant attenuation. The degree of attenuation is shown more clearly in Figure (3) where the velocimeter transfer function defined by $F_o(k_1)/F_{11}(k_1)$ has been plotted for several values of $\tilde{m}_*$, $\beta = 0.145$. Figure (4) plots the wave number at which the spectrum is reduced to half its true value (half-power point) as a function of $\tilde{m}_*$ for values of $\beta = 0.0725, 0.145, 0.29$. The curves are seen to be approximately linear on a log-log plot; clearly, the dependence on angle is diminishing as θ becomes small.

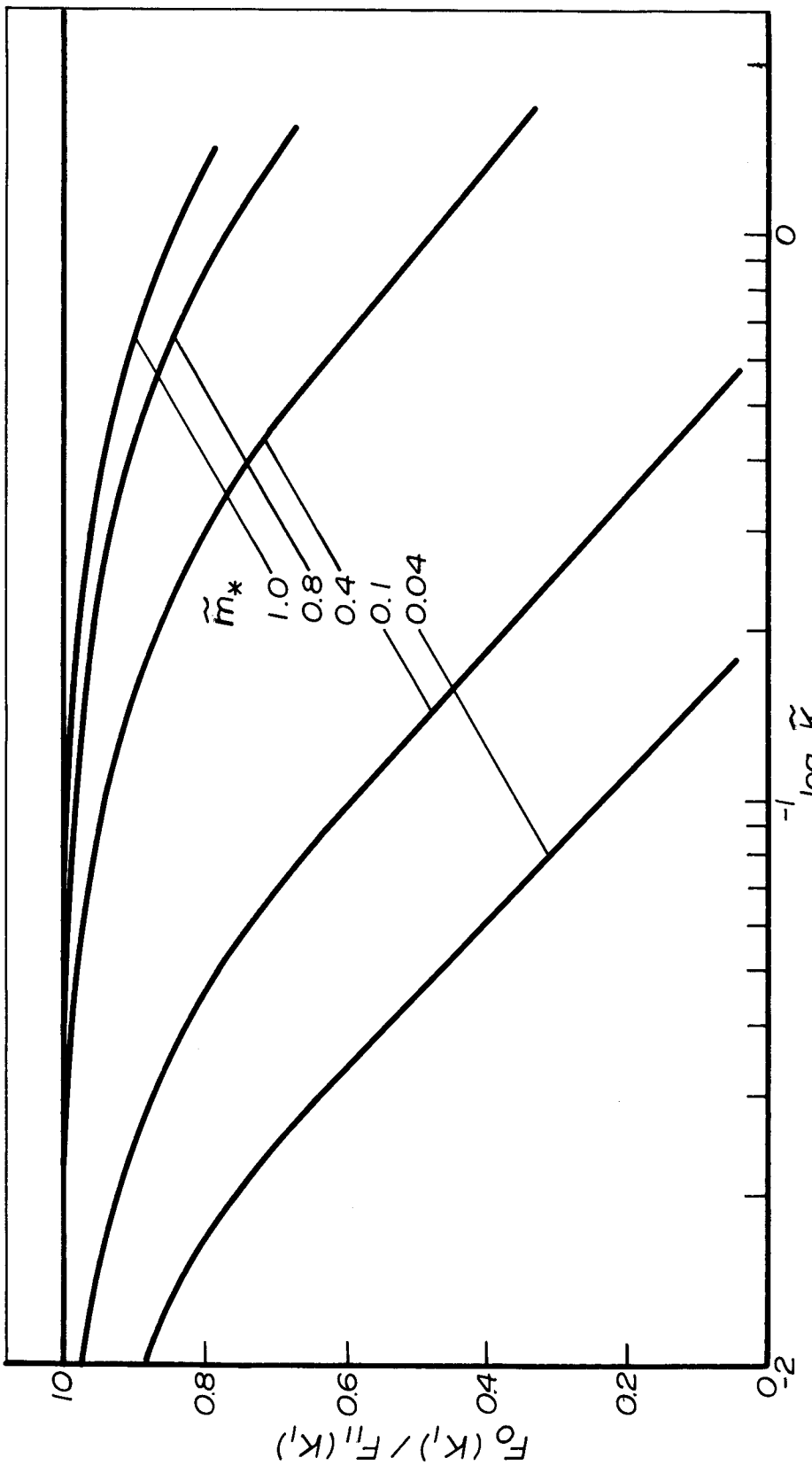

Figure 3: Scattering Volume Transfer Function F_o/F_{11}.

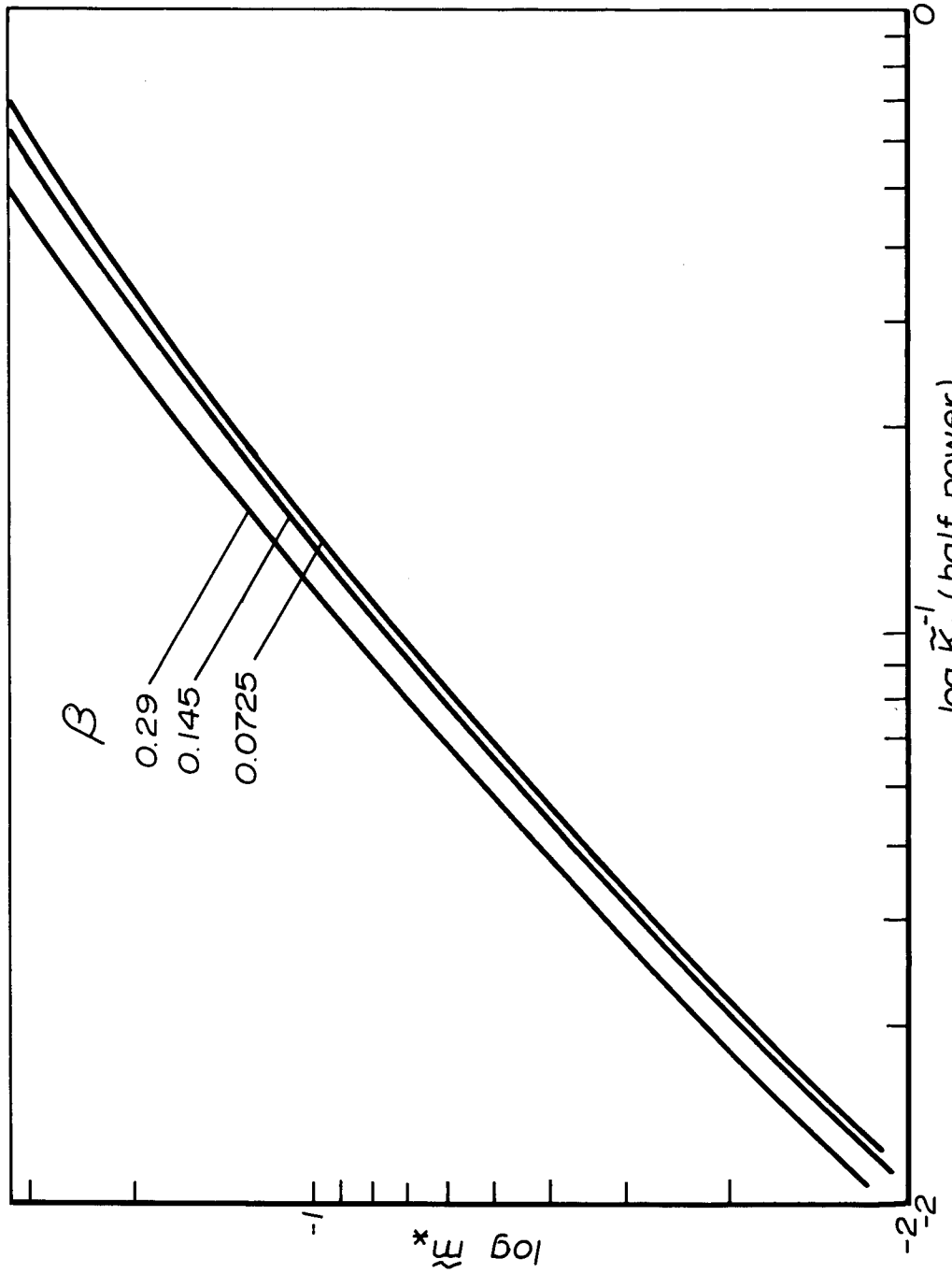

Figure 4: Wavenumber of Half Power Attenuation.

In order to illustrate more clearly the effect of the attenuation at high wave numbers the true and measured rates of dissipation, say D_T and D_m, were computed from

$$D_m/D_T = \int_{-\infty}^{\infty} k_1^2 F_o(k_1)dk_1 \Big/ \int_{-\infty}^{\infty} k_1^2 F_{11}(k_1)dk_1 \qquad (3.14)$$

D_m/D_T is shown in Figure (5) as a function of $\tilde{m}_*$. It is obvious from the graph that if the dissipation is to be measured to 10% accuracy, $\tilde{m}_*$ must be nearly unity; that is, the largest dimension of the scattering volume must be at least as small as the Kolmogorov microscale. These results are quite similar to those obtained by Wyngaard (1968) for a hot-wire and may easily be extended to the measurement of cross-stream velocity components.

3.3 *The Choice of Scattering Volume Size*

It would seem apparent from the results above that if one desires to measure the entire spectrum accurately, the smallest possible scattering volume should be used.

We shall see in Chapter 4, however, that because of the

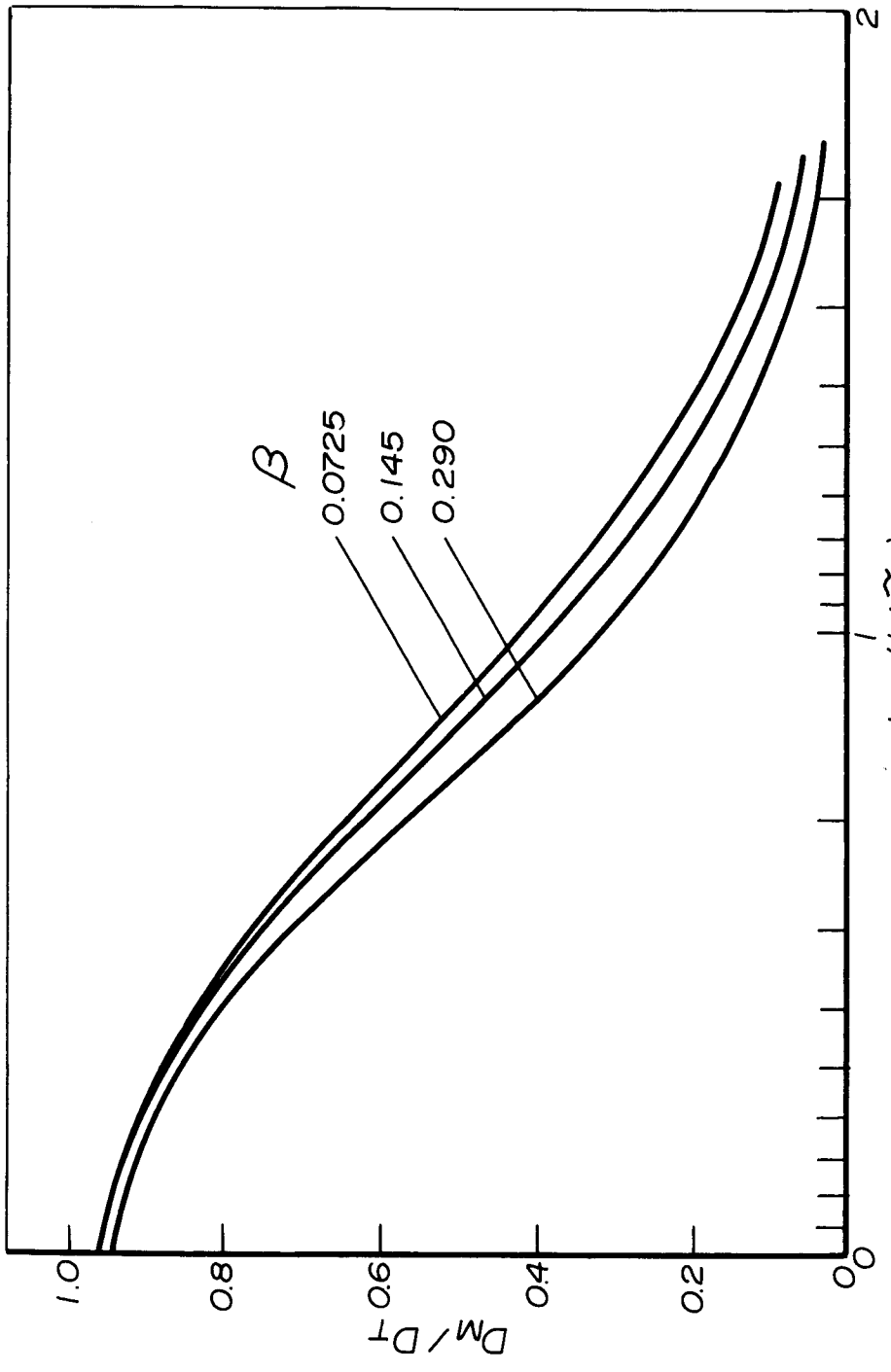

Figure 5: Ratio of Measured Dissipation to True Dissipation.

Doppler ambiguity there are very good reasons for picking a scattering volume which may be many times larger than the above criteria would indicate; clearly a trade-off will be required.

This subject will be discussed more completely in Chapter 7.

3.4 *Velocity Fluctuations Across the Scattering Volume*

It is appropriate to note at this point that because of the finite dimensions of the scattering volume, velocity gradients will exist across it; these will result in a broadening of the instantaneous Doppler signal where the amount of broadening, say $\Delta\omega_T$, will be proportional to the root mean square velocity fluctuation across the scattering volume.

The mean square fluctuating velocity across the beam is just the spatially weighted average of the quantity

$$[u(x,y,z,t) - u_o(t)]^2 \equiv (\Delta u)^2$$

It is straight-forward to show that the expected value of this quantity is given by

$$\overline{<[u(x,y,z,t) - u_o(t)]^2>} \tag{3.15}$$

$$= \int_{-\infty}^{\infty}\int\int \Phi_{11}(k_1,k_2,k_3)\{1-e^{-\{(k_1^2/2k_*^2)+(k_2^2/2m_*^2)+(k_3^2/2n_*^2)\}}\}dk_1 dk_2 dk_3$$

where — denotes the expected value and <> denotes the weighted spatial average. We may immediately recognize this from (3.6), (3.7) as

$$\overline{<(\Delta u)^2>} = \int_{-\infty}^{\infty} [F_{11}(k_1) - F_o(k_1)]dk_1 \tag{3.16}$$

and compute it as a function of (k_*,m_*,n_*) as in (3.13).

More physical insight may be gained, however, by relating $\overline{<(\Delta u)^2>}$ to the rate of dissipation ε. Expanding the exponential of (3.15) in a Taylor series we have

$$e^{-[(k_1^2/2k_*^2) + (k_2^2/2m_*^2) + (k_3^2/2n_*^2)]} \tag{3.17}$$

$$= 1 - [(k_1^2/2k_*^2) + (k_2^2/2m_*^2) + (k_3^2/2n_*^2)] + h.t.$$

Assuming that $m_*, k_*, n_* >> 0.2\,\eta^{-1}$ (the peak of the dissipation spectrum and hence the wave number associated with the velocity derivatives) and substituting (3.17) into (3.15) we have

$$\overline{<(\Delta u)^2>} \tilde{=} (1/2k_*^2)\int_{-\infty}^{\infty} k_1^2 F_{11}(k_1)dk_1 + (1/2m_*^2)\int_{-\infty}^{\infty} k_2^2 F_{22}(k_2)dk_2 + (1/2n_*^2)\int_{-\infty}^{\infty} k_3^2 F_{33}(k_3)dk_3 \tag{3.18}$$

From Batchelor (1960) we may immediately write (assuming isotropy)

$$\overline{<(\Delta u)^2>} = (\varepsilon/15\nu)[(1/2k_*^2) + (1/m_*^2) + (1/n_*^2)] \tag{3.19}$$

Since

$$m_* = n_* \sin \theta/2$$

$$k_* = n_* \cos \theta/2$$

we have

$$\overline{<(\Delta u)^2>} = (\varepsilon/15\nu)(1/m_*^2)\{1+\sin^2\theta/2[(1+2\cos\theta/2)/2\cos^2\theta/2]\}$$

$$\simeq (\varepsilon/15\nu)(1/m_*^2) \qquad (3.20)$$

because θ is usually small. The correction term, for a typical scattering angle of $\sin\theta/2 \sim 0.1$ is $\sin^2\theta/2[(1+2\cos\theta/2)/2\cos^2\theta/2] \sim 0.015$.

The Doppler bandwidth due to the turbulent velocity gradients is then given by

$$(\Delta\omega_T)^2 = (\bar{\omega}_o^2/\bar{U}^2)\overline{<[u(x,y,z,t)-u_o(t)]^2>}$$

$$\simeq (\bar{\omega}_o^2/\bar{U}^2)\ (\varepsilon/15\nu)\ (1/m_*^2) \qquad (3.21)$$

or

$$\Delta\omega_T \simeq (\bar{\omega}_o/\bar{U})\ (1/\sqrt{15}\ m_*)\ (\varepsilon/\nu)^{1/2} \qquad (3.22)$$

where $\bar{U}$, $\bar{\omega}_o$ are the mean velocity and mean Doppler frequency respectively and where $(\varepsilon/\nu)^{1/2}$ is recognized as the frequency characteristic of the turbulence fine structure. Non-dimensionalizing

by Kolmogorov variables ε,ν we have

$$\Delta\omega_T/\bar{\omega}_o = (\sqrt{1/15}\,)\,(\nu/\bar{U}\eta)\,\tilde{m}_*^{-1} \tag{3.23}$$

Thus the turbulent broadening $\Delta\omega_T$ is seen to, at least asymptotically, increase linearly with the largest dimension of the scattering volume when that dimension of the scattering volume is much smaller than the scale of the dissipative turbulent fluctuations. $\Delta\omega_T$ also depends inversely on the Reynolds number based on the mean flow rate and the Kolmogorov microscale; thus, the smaller the turbulence fine structure, the more velocity fluctuations across the scattering volume, and the greater the turbulent broadening. This is, of course, consistent with what one might have expected intuitively.

Since k_*, n_* are almost always much larger than m_* and generally chosen near $k\eta = \tilde{k} \sim 1$ where the spectrum is falling off very rapidly, another approximation to (3.15) may be obtained by ignoring the effect of k_*, n_* and integrating over k_1, k_3 to yield

$$\overline{<(\Delta u)^2>} \simeq \int_{-\infty}^{\infty} F_{22}(k_2)\{1 - e^{-k_2^2/2m_*^2}\}dk_2 \tag{3.24}$$

where $F_{22}(k_2)$ is the transverse spectrum and is defined by

$$F_{22}(k_2) = \int\int_{-\infty}^{\infty} \Phi_{11}(k_1,k_2,k_3)dk_1 dk_3 \qquad (3.25)$$

(3.24) is useful in estimating the effect of the turbulent broadening from experimentally determined spectra where the conditions for the asymptotic estimate of (3.23) may not be satisfied nor the Reynolds number sufficiently high to permit an accurate determination from Pao's spectrum as in (3.16). Clearly (3.24) reduces to (3.23) when $m_* >> 0.2\ \eta^{-1}$.

The dimensionless turbulent bandwidth defined by

$$\Delta\omega_T/\overline{\omega}_o = \sqrt{\overline{<(\Delta u)^2>}} \ / \ \overline{U} \qquad (3.26)$$

has been plotted as a function of $\tilde{m}_*$ in Figure (6). Values obtained numerically using Pao's spectrum in (3.24) and in (3.16) with $\beta = \sin\theta/2 = 0.145$ coincided within 5% and were plotted together. The asymptotic estimate of (3.23) is seen to be accurate within 10% when $\tilde{m}_* > 0.3$; for values less than this it significantly overestimates the turbulent broadening as would be expected from the form of the spectrum.

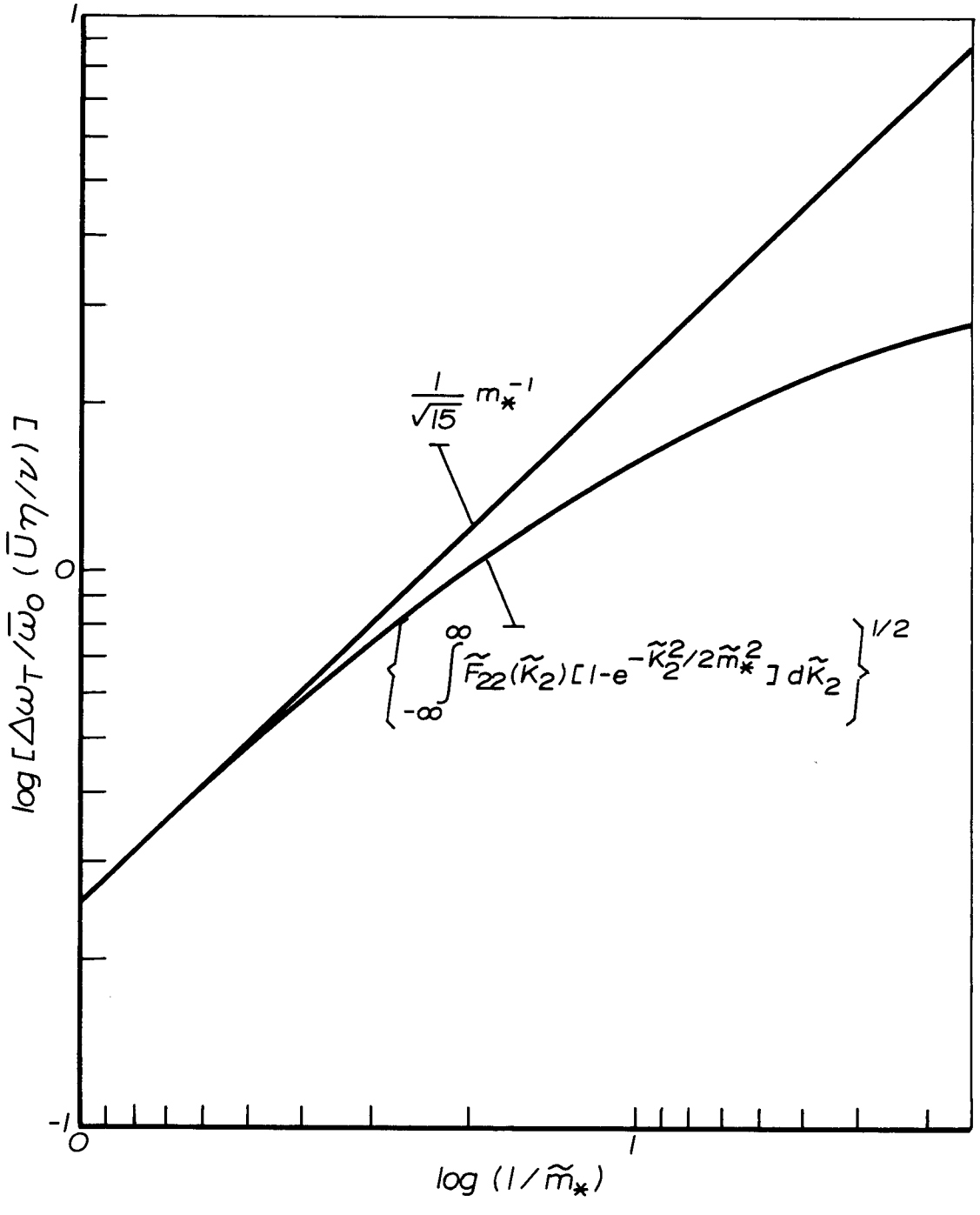

Figure 6: Dimensionless Turbulent Bandwidth.

Finally it should be emphasized that the turbulent broadening discussed above arises only from the velocity fluctuations across the scattering volume; there is, of course, additional broadening of the Doppler spectrum due to the temporal fluctuations of ω_o. This subject is discussed more fully in Chapter 4.

4.1 The Doppler Signal

The signal generated by a single scattering particle using equations (2.18) and (3.3) may be represented as

$$i_{s_p} \simeq I e^{-\{[(ut+x_o)^2/2\sigma_1^2]+(y_o^2/2\sigma_2^2)+(z_o^2/2\sigma_3^2)\}} \cos[\omega' t+\gamma(x_o)] \tag{4.1}$$

where ω' is the instantaneous Doppler frequency

$$\omega' = 2 \kappa u \sin \theta/2 \tag{4.2}$$

where $\gamma(x_o)$ is the phase

$$\gamma(x_o) = 2 \kappa x_o \sin \theta/2 \tag{4.3}$$

and where x_o is the position of the particle at $t = 0$. Recall that this representation assumes that the transit time for particles through the scattering volume is less than the smallest time scale of the turbulence; in other words, the turbulence is assumed frozen

in time as it is swept through the volume and the lateral displacement of particles is negligible.

The net signal at the photocell arising from all contributing scattering particles may be represented by

$$i(t) = \int_{\underset{\sim}{x}} i_{s_p}(t, \underset{\sim}{x}_o, \omega')\, d\xi(\underset{\sim}{x}_o) \tag{4.4}$$

$$\overline{d\xi(\underset{\sim}{x}_o)\, d\xi(\underset{\sim}{x}_o')} = \begin{cases} 0, & \underset{\sim}{x}_o \neq \underset{\sim}{x}_o' \\ d\underset{\sim}{x}_o, & \underset{\sim}{x}_o = \underset{\sim}{x}_o' \end{cases}$$

where the $d\xi(\underset{\sim}{x}_o)$ is, in fact, statistically independent at two different times and where ω' is a random variable depending linearly on the velocity. This is similar to the shot effect (c.f. Rice in Wax).

If we, as in Chapter 3, split the local Doppler frequency ω' into its average across the volume ω_o and the local deviation from ω_o, say $\omega = \omega(\underset{\sim}{x}, t)$; we may write

$$i(t) = F(t)\cos\omega_o t + G(t)\sin\omega_o t \tag{4.5}$$

where F, G are defined by

$$F(t)=I\int_{\underset{\sim}{x}_o} e^{-\{[(x_o+ut)^2/2\sigma_1^2]+(y_o/2\sigma_2^2)+(z_o^2/2\sigma_3^2)\}}\cos(\omega t+\gamma)d\xi(\underset{\sim}{x}_o) \tag{4.6}$$

$$G(t)=I\int_{\underset{\sim}{x}_o} e^{-\{[(x_o+ut)^2/2\sigma_1^2]+(y_o^2/2\sigma_2^2)+(z_o^2/2\sigma_3^2)\}}\sin(\omega t+\gamma)d\xi(\underset{\sim}{x}_o) \tag{4.7}$$

Equation (4.5) may also be written as

$$i(t) = (F^2 + G^2)^{1/2} \cos(\omega_o t - \phi) \tag{4.8}$$

where

$$\phi = \tan^{-1}\{G/F\} \tag{4.9}$$

It is straight-forward to show that if the velocity fluctuations across the scattering volume are assumed frozen in time that F and G are identically distributed Gaussian variables with correlation

$$\rho(t-t') \simeq \overline{FF'}/\overline{F^2} = \overline{GG'}/\overline{G^2} = e^{-(\Delta\omega)^2(t-t')^2/2} \tag{4.10}$$

where

$$(\Delta\omega)^2 = (\overline{U}^2/2\sigma_1^2) + (\Delta\omega_T)^2 \qquad (4.11)$$

and where we have neglected terms of order $(\Delta\omega/\omega_o)^2$ because the bandwidth of the Doppler signal is assumed small.

If there were no turbulence the Doppler bandwidth $\Delta\omega$ would be given by

$$\Delta\omega = (\overline{U}/\sqrt{2}\,\sigma_1) = k_* \overline{U} \qquad (4.12)$$

since $\Delta\omega_T$ would be zero. We may identify this with the Doppler broadening caused by the finite transit time of particles through the scattering volume and denote it by $\Delta\omega_L$; hence

$$(\Delta\omega)^2 = (\Delta\omega_L)^2 + (\Delta\omega_T)^2 \qquad (4.13)$$

The ratio $\Delta\omega_L/\omega_o$ may be easily shown to be inversely proportional to the number of Doppler pulses that are received from a single particle; clearly the more pulses that are received the lower will be the uncertainty in the determination of ω_o; this is, in fact, similar to the uncertainty principle in wave mechanics. Borrowing

from RADAR terminology, we will use the term Doppler ambiguity to denote all of the types of Doppler broadening considered here.

It should be pointed out at this time that there may be other sources of Doppler broadening which contribute to $\Delta\omega$. Clearly laminar velocity gradients will contribute to the Doppler broadening as will the presence of apertures in the optical system. We will define aperture ambiguity so as to exclude effects which may be identified as transit time phenomena and include only optical effects which cause the reception of a finite band of Doppler signals; for example, a rapidly diverging or converging scattering beam which causes a varying scattering angle across the scattering volume. If we assume that the velocity gradients and apertures are Gaussian, for convenience, it is easy to show that the total bandwidth is given by

$$(\Delta\omega)^2 = (\Delta\omega_L)^2 + (\Delta\omega_T)^2 + (\Delta\omega_G)^2 + (\Delta\omega_A)^2 + (\Delta\omega_B)^2$$

where $\Delta\omega_G$ is the bandwidth associated with the laminar velocity gradient, $\Delta\omega_A$ is the aperture-induced bandwidth, and $\Delta\omega_B$ includes the possible broadening due to an nonmonochromatic light source.

In the remaining analysis of this work, we shall consider only the broadening due to the finite transit time and the turbulence; however, the extension to the general case is straight-forward.

4.2 *The Spectrum of the Doppler Signal and Intensity Measurements*

The spectrum of equation (4.8) is easily obtained as

$$F(\omega) = (1/\sqrt{8\pi}\ \Delta\omega)\{e^{-(\omega-\omega_o)^2/2(\Delta\omega)^2} + e^{-(\omega+\omega_o)^2/2(\Delta\omega)^2}\} \qquad (4.14)$$

This is obviously the sum of two Gaussian peaks centered at $\pm\omega_o$. In turbulent flow the center frequencies $\pm\omega_o$ are also fluctuating yielding an additional broadening equal to the root mean square fluctuation of ω_o; in fact,

$$F_T(\omega) = \int_{-\infty}^{\infty} F(\omega-\omega_o)\ P(\omega_o)d\omega_o \qquad (4.15)$$

where $P(\omega_o)$ is the probability density of ω_o.

Clearly, the foregoing analysis must be taken into consideration whenever one attempts to measure mean square fluctuating quantities from the spectrum of the Doppler signal; when the fluctuations of ω_o are of order $\Delta\omega$ the fluctuating velocities can no longer be distinguished from the fluctuations due to the Doppler ambiguity. The problem is illustrated graphically in Figure (7).

The limit of resolution may be taken as

$$\Delta\omega/\overline{\omega}_o \quad < \quad u'/\overline{U} \qquad (4.16)$$

where u' is the root mean square fluctuating velocity. It should be noted that because of the turbulent broadening $\Delta\omega_T$, the intensity values measured from the spectral broadening may not be corrected by simply subtracting the values measured in laminar flow as suggested by some authors (Pike et al (1967), Goldstein (1967)). Failure to properly account for the Doppler ambiguity may explain the anomalous results of Greated (1969).

4.3 *Instantaneous Velocity Measurements*

The matter of measuring instantaneous fluctuating velocities

is somewhat more serious and involves the question of the spectrum of the fluctuations in phase. From equation (4.8) we have

$$i(t) = (F^2 + G^2)^{1/2} \cos(\omega_o t - \phi)$$

The usual sort of measuring circuit will remove the amplitude information by amplifying and clipping, keeping only the information on the zero crossings, and will produce a signal proportional to frequency

$$\omega_1 = \omega_o - d\phi/dt \tag{4.17}$$

We write

$$\omega_o = \int e^{i\alpha t} dZ(\alpha) \qquad \overline{dZ(\alpha)dZ(\alpha')} = \begin{cases} 0, & \alpha \neq \alpha' \\ (\bar{\omega}_o^2/\bar{U}^2) F_o(\alpha/\bar{U}) d(\alpha/\bar{U}), & \alpha = \alpha' \end{cases} \tag{4.18}$$

$$\dot{\phi} = \int e^{i\alpha t} dN(\alpha) \qquad \overline{dN(\alpha)dN(\alpha')} = \begin{cases} 0, & \alpha \neq \alpha' \\ \eta(\alpha)d\alpha, & \alpha = \alpha' \end{cases} \tag{4.19}$$

where $\bar{\omega}_o$ is the expected value of the mean center frequency

corresponding to the mean flow velocity $\overline{U}$, F_o is the spectrum of u_o, the volume averaged velocity defined in Chapter (3), and $\eta(\alpha)$ is the spectrum of the phase fluctuations. Clearly

$$\omega_1 = \int e^{i\alpha t} dZ(\alpha) - \int e^{i\alpha t} dN(\alpha) \tag{4.20}$$

and since the phase fluctuations and ω_o are uncorrelated, the spectrum of the composite signal is given by

$$(\overline{\omega}_o^{\,2}/\overline{U}^{3}) F_o(\alpha/\overline{U}) + \eta(\alpha) \tag{4.21}$$

4.4 *The Measurement of Turbulent Spectra*

The problem of measuring turbulent spectra has thus been reduced to what is $\eta(\alpha)$. Since F and G are identically distributed Gaussian random variables, we may take F and G to be the coordinates of a point in the x-y plane where the point moves in such a way that it has a circularly symmetric Gaussian distribution. ϕ is clearly the angle subtended by the radius vector and the x-axis.

It is evident that ϕ is not stationary. If ϕ begins from zero, say, then for times short compared to $2\pi/\Delta\omega$ the probability of finding $|\phi| > 2\pi$ will be small; as time passes it becomes more and more likely that ϕ will have made one or more revolutions about the origin. The value of the spectrum at the origin is given by

$$\eta(o) = (1/2\pi) \int_{-\infty}^{\infty} \overline{\dot{\phi}(t)\dot{\phi}(t+\tau)}d\tau = (1/2\pi)\ \overline{d\phi^2/dt} \qquad (4.22)$$

This will be non-zero since ϕ is nonstationary.

The joint characteristic functional of F and G is determined entirely by one parameter $\Delta\omega$; consequently that of ϕ will also be determined only by $\Delta\omega$. Hence we must have on dimensional grounds

$$\overline{d\phi^2/dt} \propto \Delta\omega \qquad (4.23)$$

with an unknown coefficient, hopefully on order unity.

The exact form of the spectrum has been determined analytically in Appendix (2). The coefficient in equation (4.23) is equal to 2π and the spectrum is flat to $\alpha \sim \Delta\omega$ beyond which it drops slowly as

inverse frequency. Since $\alpha \sim \Delta\omega$ is usually beyond the cutoff of the electronics, the spectrum is experimentally white with height $\Delta\omega$; i.e.,

$$\eta(\alpha) \cong \Delta\omega \tag{4.24}$$

If there is a significant amount of noise added by the electronics and the detection process, this will also contribute to the random phase fluctuations. The effect of a filtered white noise on the spectrum $\eta(\alpha)$ is included in the analysis of Appendix (2). If β is taken as the signal-to-noise ratio measured after the filter and $\Delta\omega_f$ is the filter half-width, the spectrum of the phase fluctuations is increased by the ratio

$$1 + 0.40(\Delta\omega_f/\Delta\omega\beta^2)$$

where it is assumed that $(\Delta\omega_f/\Delta\omega\beta^2) < 1$ and $(\Delta\omega_f/\Delta\omega)^2 >> 1$.

The spectrum of the Doppler ambiguity plus noise is then given by

$$\eta(o) \simeq \Delta\omega \{1 + 0.40(\Delta\omega_f/\Delta\omega\beta^2)\} \tag{4.25}$$

It is easily seen that the effect of the noise is to set a lower bound on the minimum spectral height that can be achieved by reducing $\Delta\omega$ while keeping the signal-to-noise ratio β constant.

4.5 *The Limit of Spectral Measurement*

The limit of measurement of $F_{11}(\alpha)$ will be determined by the frequency α_o where the ratio of the turbulence spectrum to the ambiguity spectrum is unity, or where

$$(\bar{\omega}_o^{\,2}/\bar{U}^3)F_{11}(\alpha_o/\bar{U}) = \eta(\alpha_o) \tag{4.26}$$

Nondimensionalizing by Kolmogorov variables ε,ν

$$\begin{aligned} &\alpha_o\eta/\bar{U} = \tilde{k}_o \qquad k_*\eta = \tilde{k}_* \\ &F_{11}(\alpha_o/\bar{U}) = \varepsilon^{1/4}\nu^{5/4}\tilde{F}_{11}(\tilde{k}_o) \end{aligned} \tag{4.27}$$

where η is the Kolmogorov microscale

$$\eta = (\nu^3/\varepsilon)^{1/4}$$

we have, using (4.13) for $\Delta\omega$ and the asymptotic estimate for $\Delta\omega_T$ given in equation (3.23)

$$\tilde{F}_{11}(\tilde{k}_o) = 2.53 \times 10^{-2}\tilde{k}_*R^2\{1+[(2\pi)^2/15R^2\tilde{k}_*^4\sin^2\theta/2]\}^{1/2} + 2.53 \times 10^{-2}\tilde{k}_*R^2(0.4\,\Delta\omega_f/\Delta\omega\beta^2) \tag{4.28}$$

where the first term includes the effects of transit time and turbulence broadening respectively and the second term is the effect of the photodetection noise from equation (4.25). The parameter R is defined by

$$R = 2\pi\bar{U}^2/\nu\bar{\omega}_o = \bar{U}\lambda/\nu 2\sin\theta/2 \tag{4.29}$$

Physically, R is just a Reynolds number based on the smallest length that can be resolved in the mean flow direction; if the crests of the light waves (wave length λ) make an angle $\theta/2$ with the direction of mean flow, then $\lambda/2\sin\theta/2$ is the smallest length that can be resolved in that direction.

If we ignore the contribution of the noise, the lowest ambiguity spectral level (highest cutoff frequency α_o) is obtained when the contributions of the turbulence and the transit time are equal; from (4.28) the optimum cutoff wave number is then

$$\tilde{k}_{*crit.} = 1.27(R \sin \theta/2)^{-1/2} \tag{4.30}$$

Thus the lowest ambiguity spectral height for fixed R and θ is given by

$$F_{11}(\tilde{k}_o) = 4.27 \times 10^{-2} R^{3/2}/(\sin \theta/2)^{1/2} \tag{4.31}$$

This equation implicitly determines the largest $\tilde{k}_o$ (the wave number of unity turbulence to ambiguity spectrum) that can be obtained for fixed R and θ.

The ambiguity spectral levels from equation (4.28) are shown in Figures (8) and (9). Figure (8) shows the relative effect of the photodetection noise as a function of $\beta/\sqrt{\Delta\omega_f/\Delta\omega}$. Figure (9) demonstrates the combined effects of the finite transit time and turbulence broadening as a function of $\tilde{k}_*/\tilde{k}_{*crit.}$ for R = 1.0, sin $\theta/2$ = 0.1.

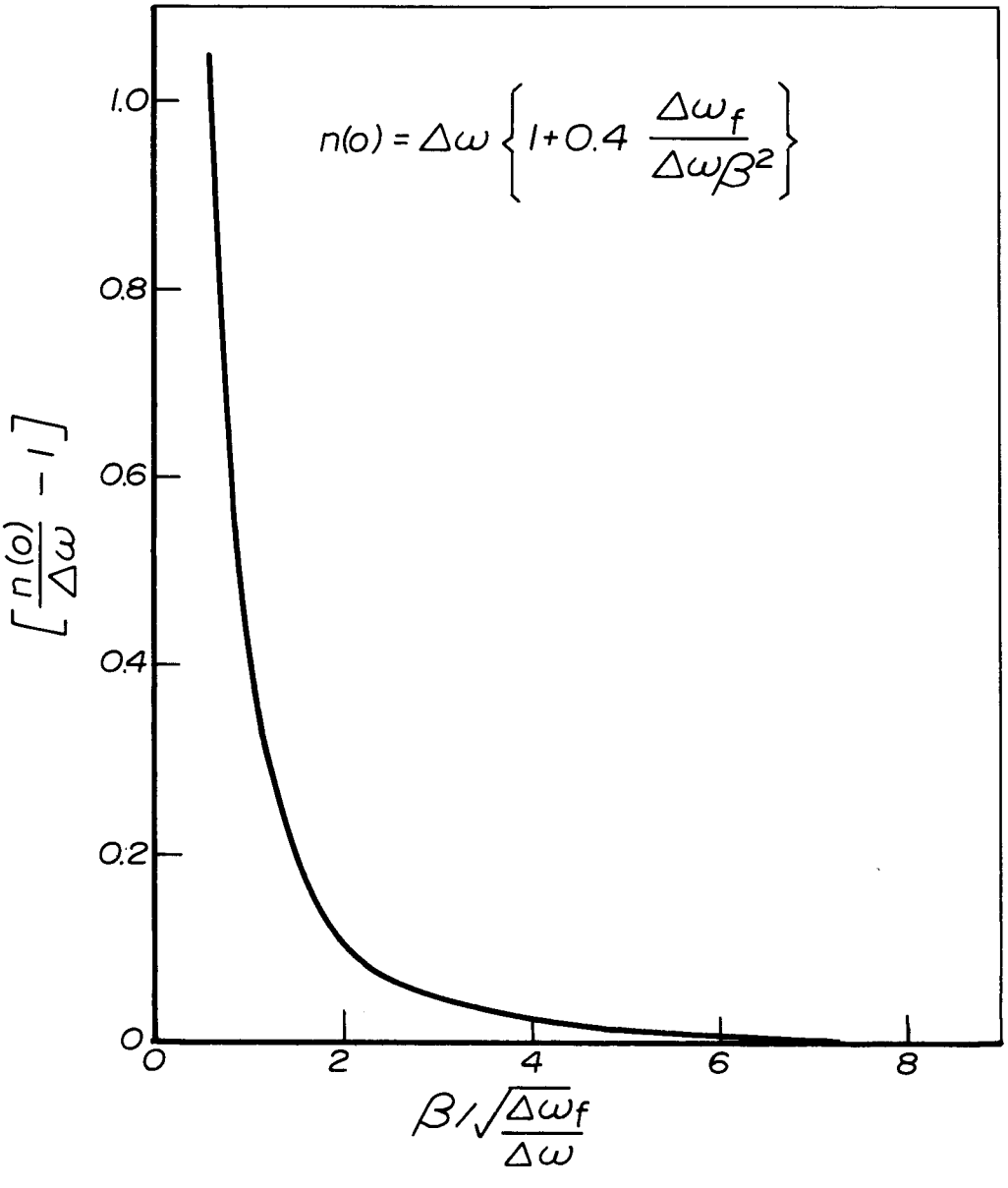

Figure 8: Relative Influence of the Electronic Noise on the Ambiguity Spectrum.

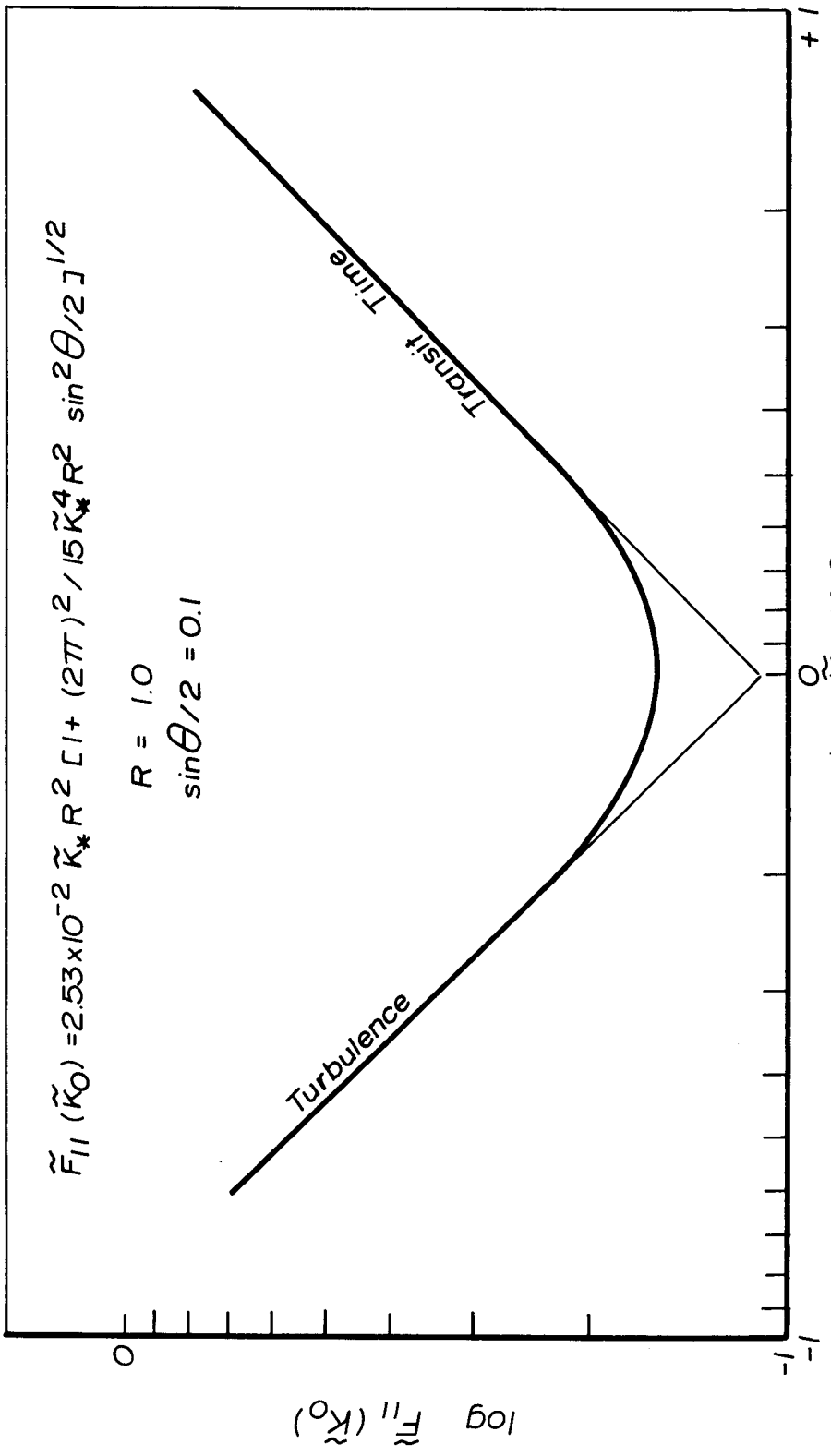

Figure 9: Spectrum of Combined Transit Time and Turbulent Ambiguity.

The optimum spectra from equation (4.31) are shown in Figure (10) for several values of $R_1 = R/(\sin \theta/2)^{1/3}$. Pao's spectrum for the turbulence has also been plotted; $\tilde{k}_o$ is determined by the intersection of the turbulence and ambiguity spectra.

Finally, Figure (11) shows $\tilde{k}_o$ (unity turbulence spectrum to ambiguity spectrum) as a function of R_1. $\tilde{k}_o$ is determined implicitly by equation (4.31) and Pao's spectrum has been used for $\tilde{F}_{11}(\tilde{k}_o)$.

From Figure (11) it can be seen that for $\tilde{k}_o = 1$, $R(\sin \theta/2)^{1/3} = 0.10$. With typical values of $\lambda = 6.3 \times 10^{-5}$ cm., $\nu = 10^{-2}$ cm^2/sec (corresponding to measurements in water) and $2 \sin \theta/2 = 0.2$ we have

$$\overline{U} \sim 1.5 \text{ cm/sec}$$

Relaxation of the resolution requirements to $\tilde{k}_o = 0.1$ increases the permissible mean velocity $\overline{U}$ by about two orders of magnitude. It should be remembered, however, that the $\tilde{k}_o$ determined from equation (4.28) is actually quite conservative since a turbulence/ambiguity ratio of unity does not permit accurate determination of the spectrum.

From Figure (10) it can be seen that for $\tilde{k}_o \sim 1$, the spectrum begins to deviate perceptably at about $\tilde{k}_o \sim 0.5$. A certain amount of subtraction of the ambiguity can be done since it is uncorrelated with the turbulence.

The situation might be improved somewhat by increasing the mean Doppler frequency $\bar{\omega}_o$ which corresponds to increasing the scattering angle θ. Unfortunately, forward scattering is much more efficient and it is difficult in practice to achieve a suitable Doppler signal when $2 \sin \theta/2$ is much above 0.7. Additional problems may arise from the electronics as higher frequencies are used.

4.6 *Intensity Measurements and Higher Order Statistics*

From the form of $\eta(\alpha)$ and from Appendix (2), the mean square value of $\dot{\phi}$ is infinite. This value in practice is finite because of the low-pass filtering introduced by the detection process; however, considerable contamination of intensity measurements from the instantaneous signal may result because of the wide band nature of $\dot{\phi}$. Clearly this effect will also be present and perhaps even dominant in attempts to measure higher order statistics such as skewness and kurtosis.

4.7 *Two-Point Velocity Correlations*

Two-point velocity correlations may be performed using two independent Laser-Doppler Velocimeters. From equation (4.4) it is clear that as long as the scattering volumes do not overlap, the Doppler ambiguity induced phase fluctuations are uncorrelated between the two signals; consequently, only velocity correlations are obtained, i.e.,

$$\begin{aligned} \overline{\omega^{(1)}\omega^{(2)}} &= \overline{\omega_o^{(1)}\omega_o^{(2)}} + \overline{\dot{\phi}^{(1)}\dot{\phi}^{(2)}} \\ &= \overline{\omega_o^{(1)}\omega_o^{(2)}} \\ &= (\overline{\omega}_o^{\,2}/\overline{U}^2)\ \overline{u^{(1)}u^{(2)}} \end{aligned} \tag{4.32}$$

where (1) and (2) denote the signals from the two velocimeters. This is consistent with the observations of Clarke (1970) who successfully measured velocity correlations in turbulent pipe flow by using two velocimeters.

It has been suggested (Morton (1970)) that the phase fluctuations from two velocimeters looking at the same scattering

volume might be uncorrelated if the velocimeters were placed at different angles to the flow (i.e., rotated about the axis defined by the mean flow direction) because the phases for individual particles would be different. An examination of equations (4.3) and (4.4) reveals that the phase of a scattering particle depends only on the x-coordinate which is the same for each velocimeter. Thus, while the correlation may not be unity because of the possibly different amplitudes associated with each particle, it clearly will be finite if the scattering volumes indeed overlap.

4.8 *Summary*

The effect of the Doppler ambiguity on attempts to measure turbulence has been examined. The ambiguity was seen to arise from the finite transit time of particles through the scattering volume as well as from velocity gradients across the beam. The additional random phase fluctuations due to electronic noise were also considered.

The random phase fluctuations were seen to influence spectral measurements at all frequencies, as well as providing a major source of error in attempts to measure the higher order statistics of

the turbulence. Criteria for minimizing the Doppler ambiguity were established. In Chapter 7, we shall examine these criteria in conjunction with the resolution criteria of Chapter 3.

5 EXPERIMENTAL APPARATUS

5.1 Introduction

This chapter attempts to briefly describe the apparatus used in obtaining the experimental results which are presented in Chapter 6. Included are descriptions of the optics, the heterodyne receiver, the flow facility, and the signal processing units.

5.2 The Optical System

The optical system used in these experiments is of the type proposed by Goldstein and is shown in Figure (12). The system was chosen for its simplicity and for the ease with which it could be aligned.

The source of radiation was a nominal 50 mw. Ne-He Laser (Spectra-Physics Model 125); the actual output was closer to 90 mw. The beam was vertically polarized and of Gaussian cross-section. The distance between the $1/e^2$ points of intensity was about 2 mm. and the divergence angle was less than 0.7 millirad.

The beam was split into the reference and scattered beams by means of a polarized beamsplitter which passed only horizontally polarized light. By rotating the plane of polarization of the incoming light with a polarization rotator (Spectra-Physics Model 310), the relative intensity of the two beams could be adjusted for the optimum signal strength. A second polarization rotator served to return the horizontally polarized beam to vertical since the scattering intensity is maximized when the polarization of the light is perpendicular to the plane of scattering (which in our case was horizontal).

The two beams were focused to the desired region in the flow with spherical lenses obtained from Ealing Optical. Since the f-number based on beam diameter in our experiments ranged from 50 to 1000, aberations were negligible and the lenses were diffraction limited to a high approximation. Precise alignment was afforded by micrometer mirror mounts (Oriel Model 145) in the reference and scattered beams.

The entire optical system rested on a 700 lb. concrete table supported by four viscoelastic sandwich pads. This arrangement served to minimize vibrations to the point where no realignment of the optics was necessary over run periods up to three hours.

The test section was circular in cross-section and constructed of plexiglass tubing. To minimize the lens effect of the test section, an optically flat box was placed around the test section and filled with water so as to provide an approximately constant index of refraction. No additional optical filters or apertures were present between the flow and the photodiode.

5.3 *The Scattering Agent*

Because of the large quantity of scattering particles necessary for a 1000 gallon facility, an inexpensive supply was necessary. Homogenized milk in concentrations of about 1: 2000 was found to provide an excellent signal-to-noise ratio. From Clayton, the average fat particle size is approximately 0.3 microns with about 10^{14} particles per liter of milk. The primary disadvantage of milk was, of course, the necessity of frequently draining the facility.

5.4 *The Optical Receiver*

The heart of the receiver package was an EG & G Model SDG-040A

photodiode (surface area ~ 0.1 cm^2). This was chosen because of its high quantum efficiency (~ 50%) and low cost (~ $15.00). The photodiode was biased at 90 v. with standard mercury cells. The noise was primarily due to the input noise from the first amplifier stage; this represented a distinct improvement over previous attempts to use a photomultiplier tube where because of the much lower quantum efficiency the noise was predominantly photon shot noise from the reference beam. With utilization of the latest avalanche and combination diodes, the noise in our setup could probably have been reduced to the shot noise limit, but this was not deemed necessary.

The photodiode was followed by a single broadband amplifier having a gain of 12, a tunable bandpass filter (250 to 700 kHz) with a bandwidth of about 10%, and an infinite clipper (gain ~ 140 db.) which effectively removed all the amplitude information. Signal-to-noise ratios measured after the filter by blocking the scattering beam typically ranged from 10 to 50.

5.5 *Frequency-to-Voltage Convertor*

The frequency-to-voltage convertor, together with the optical

receiver package, is shown in Figure (13). The F-to-V convertor was constructed from standard Honeywell 5 mc. microcircuits (μ-PACS) along with a -60 db/octave Butterworth low pass filter (Wyngaard, et al (1967)). The response was linear to inputs between 8 kHz and 1 MHz to within 3%.

5.6 *The Flow Facility*

The facility used in these experiments is shown diagrammatically in Figure (14). It is essentially a closed circuit water tunnel with a 1.7 inch I.D. circular test section. The flow passes from a 1000 gallon reservoir into a 12" diameter by 30" long settling chamber. From the settling chamber the flow enters the test section through a 36:1 contraction. The flow is pulled through the test section by a pump which permits flow rates up to 10 meters per second; the flow rate is controlled by varying the pump speed or by adjusting the valve in the return system. The mean flow rate shows negligible drift over periods up to an hour and the root mean square velocity fluctuation with no grid is less than 0.2% of the mean flow rate.

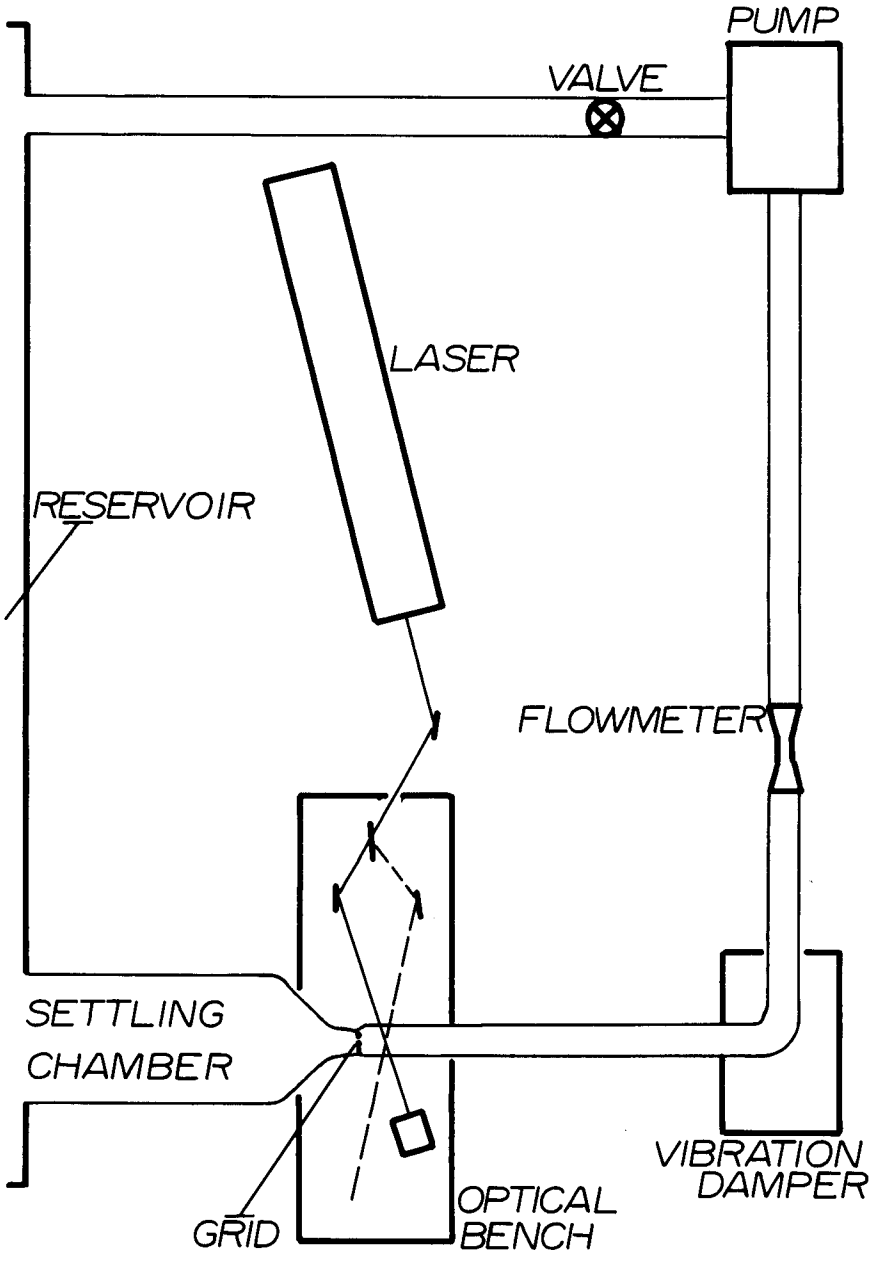

Figure 14: Flow Facility

The flow could be made turbulent by means of a grid inserted at the end of the contraction. The grid was of biplane design and was constructed of #19 hypodermic needle tubing. The bar spacing was 0.1 "; this corresponded to a solidity of 0.32 which was close to that used by other investigators of homogeneous turbulent flows (c.f. Corrsin, et al (1966)).

5.7 *The Measurement of Mean Flow Rate*

Mean flow velocities were measured with a Potter flowmeter (Model 1-5550) which was installed after the test section. The meter produced a signal whose frequency was proportional to the mean flow rate. The frequency of the flowmeter output was monitored with a counter and flow rates were read from the calibration curve which was linear over the range of velocities used.

5.8 *The Measurement of Spectra*

A block diagram of the spectral measuring equipment is shown in Figure (15). The amplitude-modulated signal from the detector

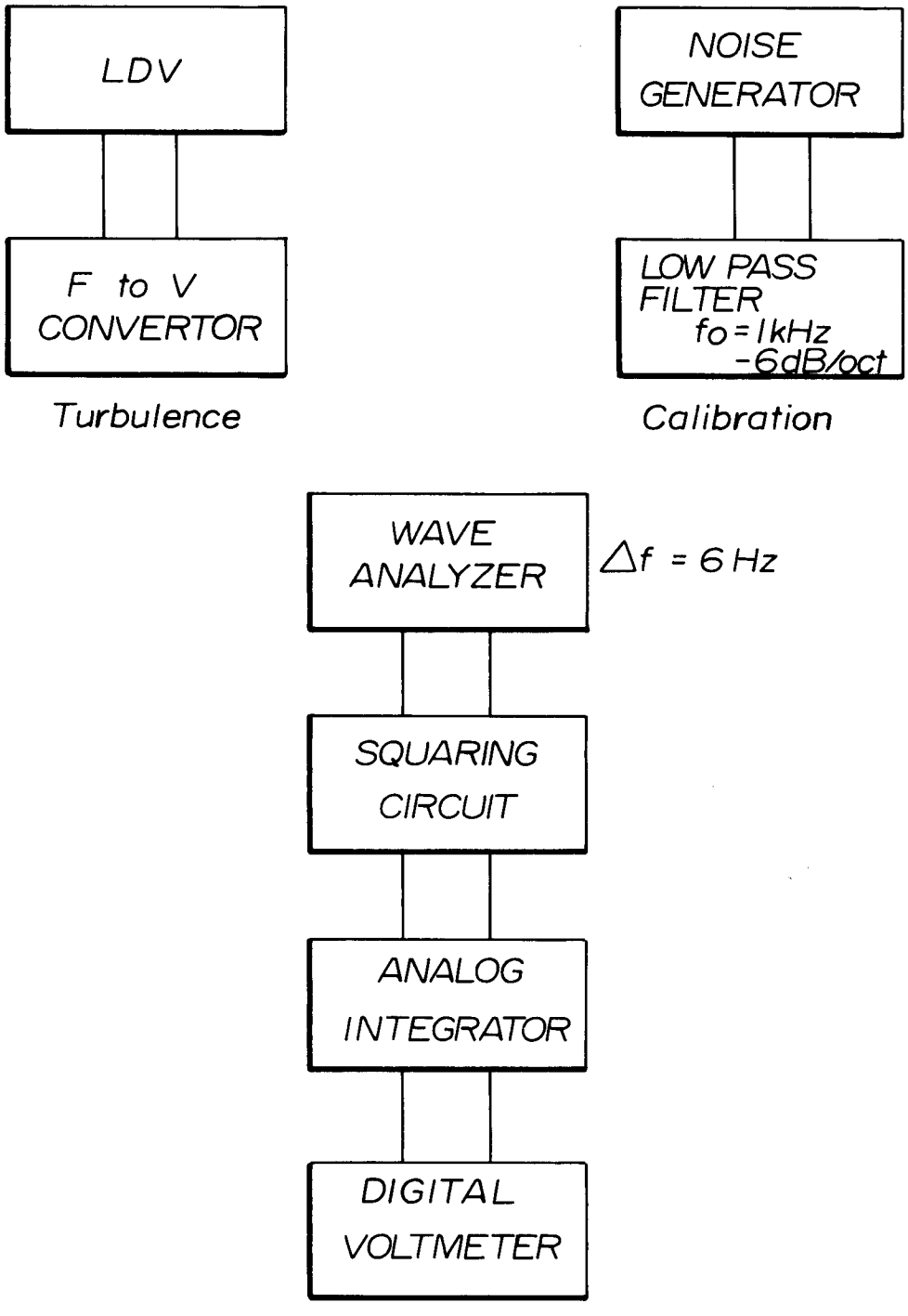

Figure 15: Setup Used for the Measurement of Spectra.

of the Laser-Doppler Velocimeter was fed into a Hewlett-Packard Model (302A) Wave Analyzer (equivalent noise bandwidth 6 cps.). The internal 100 kHz carrier from the wave analyzer was squared by a Ballantine true r.m.s. voltmeter (Model 320A) and then integrated for 60 seconds by an analog integrator which yielded a D.C. output proportional to the spectral height.

The system was calibrated with a random noise generator (Scott Model 811-A) as shown also in Figure (15). The spectrally white output from the generator was filtered by a 6 db/octave low pass filter and the height of the spectrum for some frequency well below the filter cutoff was measured. It is not difficult to show that if f_o is the frequency of the 3 db. point of the filter, $\overline{e^2}$ is the mean square value of the filtered output from the noise generator, A is the true spectral height, and A_{meas} is the measured spectral height, then

$$A = CA_{meas} = \frac{\overline{e^2}}{\pi f_o}$$

where C is the calibration constant.

5.9 *Experimental Error*

If it is assumed that the experimental error is due primarily to the fact that we are taking a finite sample of a random signal, we may estimate the error if we assume that the input is Gaussian. The error E, defined by the root mean square fluctuation from the expected value, for spectral measurements is given by Lumley (1964) as

$$E^2 = \sqrt{2}\,/T\Delta f$$

where Δf is the bandwidth of the analyzer and T is the averaging time. Using a Δf of 6 cps. and an integration time of 60 seconds, we have

$$E^2 = \sqrt{2}\,/60 \times 6$$

or

$$E = 0.06$$

Thus the spectral measurements may be believed to about 6%. Since the spectral calibration described earlier has the same level of confidence, a reasonable estimate of the overall error would not be worse than 12%.

6 EXPERIMENTAL RESULTS

6.1 Introduction

Spectral measurements were taken in both laminar and turbulent flow in water in an attempt to identify the separate effects of finite particle transit time and the turbulent fluctuations across the beam. In all cases the effect of the noise was less than 1%.

The flow velocities varied from 70-100 cm/s and the Doppler beat frequencies from 250-650 kHz. This corresponded to values of R from about 1 to 3.

6.2 Laminar Flow

Figure (16) shows measured spectra in laminar flow. The measurements were non-dimensionalized by a nominal value of $\nu = 10^{-2}$ cm^2/s and the cutoff wave number k_* (since without turbulence there is no η) which was computed from equations (2.15) and (3.5). The dependence of the height of the ambiguity spectrum on the transit time $(1/k_*\bar{U})$ is clearly shown in Figure (17) which plots spectral height as a function of k_*. Agreement with theory

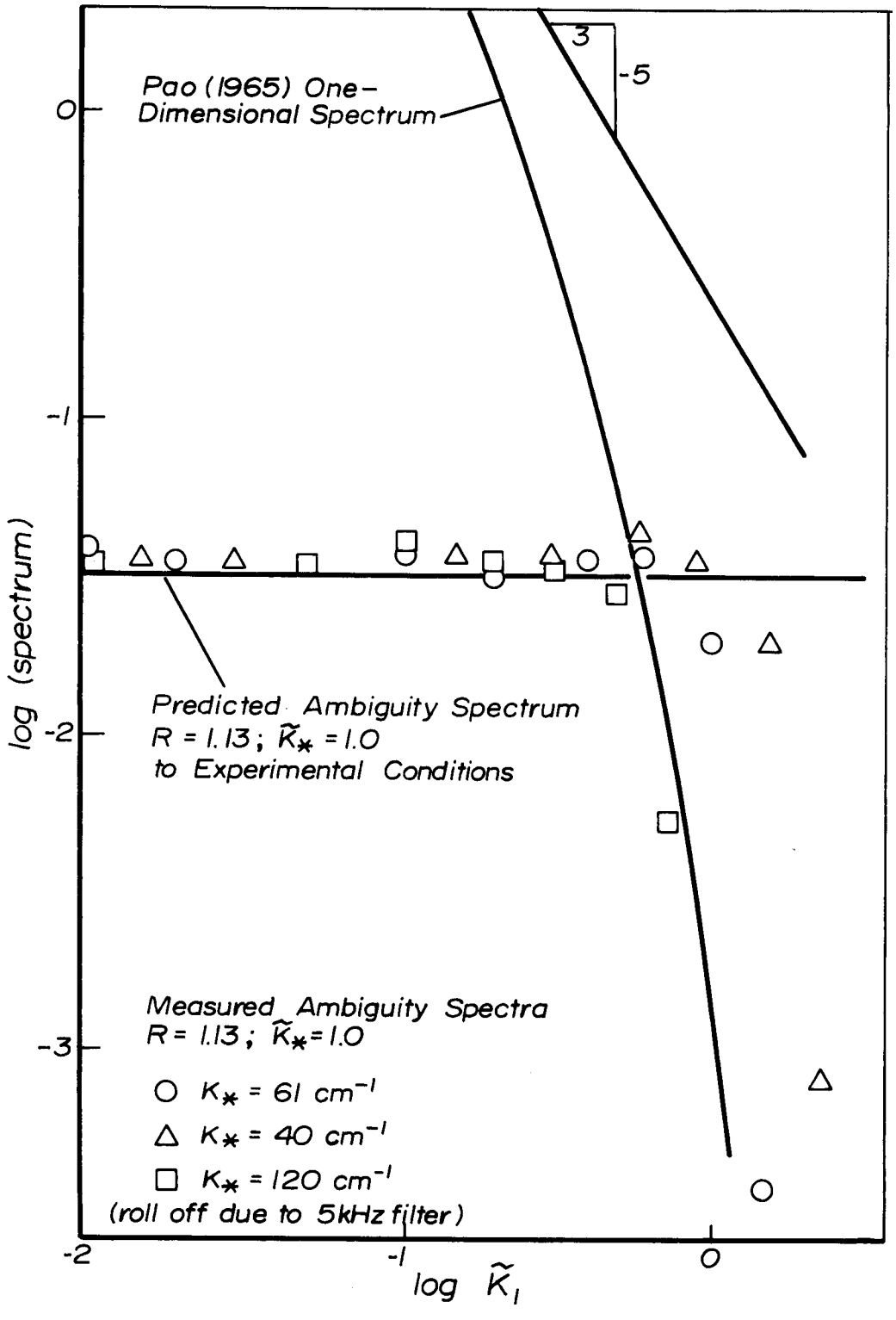

Figure 16: Comparison of Predicted and Measured Spectra in Laminar Flow.

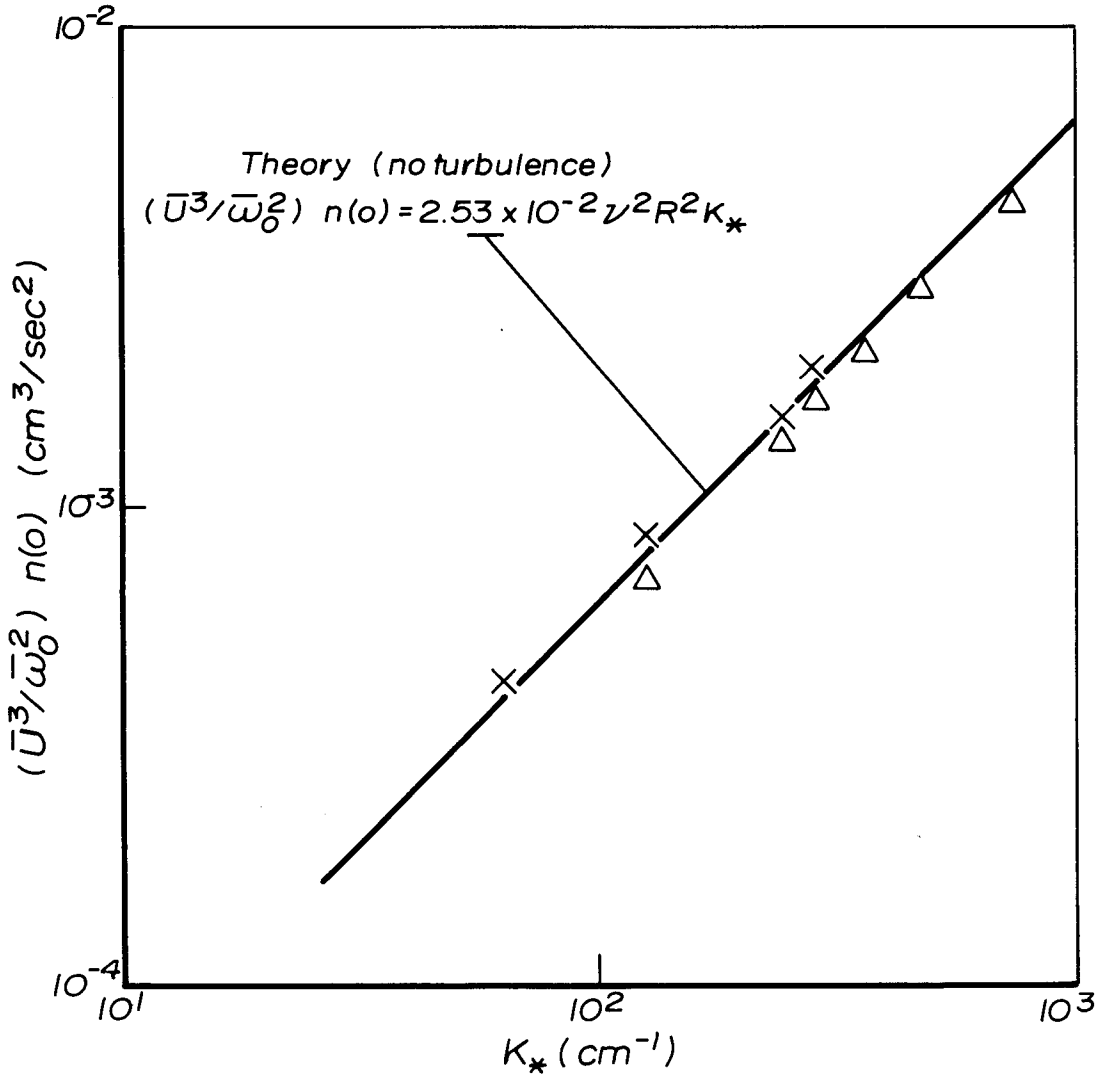

Figure 17: Measured Spectral Height in Laminar Flow (R=1.6).

is seen to be within 10% although one set of measurements in Figure (17) is seen to be consistently low (about 10-15%). This would not be considered significant were it not for the fact that measurements in turbulent flow show about the same discrepancy.

6.3 *Turbulent Flow*

The measurements in turbulent flow were taken at 45 mesh lengths behind the grid where the turbulence is approximately isotropic. Spectra were non-dimensionalized by ν and the rate of dissipation ε determined from the measured decrease in turbulent intensity with distance from the grid. The intensity measurements were taken with a hot-film anemometer because of the high ambiguity to turbulence ratio in such a low intensity flow.

A typical turbulence spectrum is shown in Figure (18). The measured spectral values are seen to approach a constant value and then to drop slowly; the constant value is within 10% of that predicted theoretically and the slow drop-off seems to begin at about the wave number corresponding to $\alpha \sim \Delta\omega$ as predicted. The constant value was subtracted from the measured spectral values;

the result is seen to be close to Pao's spectrum although about 10% above it. The error may be due to an error in the calibration of the measurements.

Corrected spectral measurements for six different values of $\tilde{k}_*$ are shown in Figure (19). The smallest value of $\tilde{k}_*$ used (0.55) corresponds to a value of $\tilde{m}_* = 0.08$. Clearly, as expected from the analysis of Chapter 3, this set of measurements shows considerable attenuation (~ 50%) at all wave numbers. Because of the low Reynolds number (deviation from Pao's spectrum at low wave numbers) and the large error at high wave numbers, it was not possible to perform an accurate check on the transfer function given in Chapter 3.

Figure (20) shows the measured ambiguity spectral height (determined from the asymptotic values of the turbulent spectra) as a function of $\tilde{k}_*/\tilde{k}_{*crit}$ where $\tilde{k}_{*crit}$ is computed from equation (4.30). The asymptotic theory is *not* applicable here because of the relatively small values of $\tilde{m}_*$. Likewise, the turbulent bandwidth computed from Pao's spectrum is too high since it is clear from the measured spectra that the velocity fluctuations at low wave numbers are overestimated. The transverse spectrum $F_{22}(k_2)$ was computed from the measured longitudinal spectrum $F_{11}(k_1)$ and this was used in equation (3.24) to compute the turbulent bandwidth $\Delta\omega_T$.

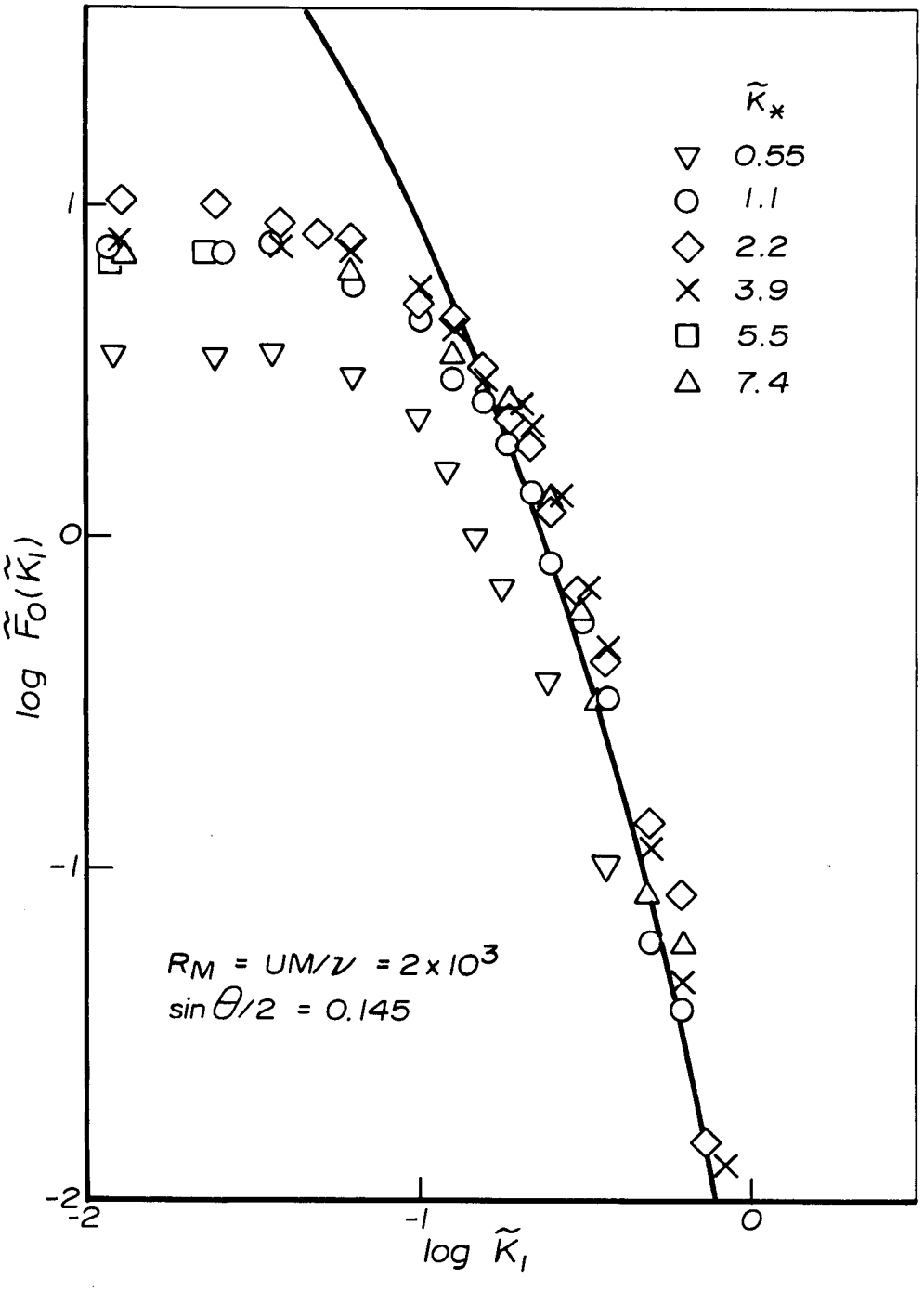

Figure 19: Turbulence Spectra with Ambiguity Subtracted.

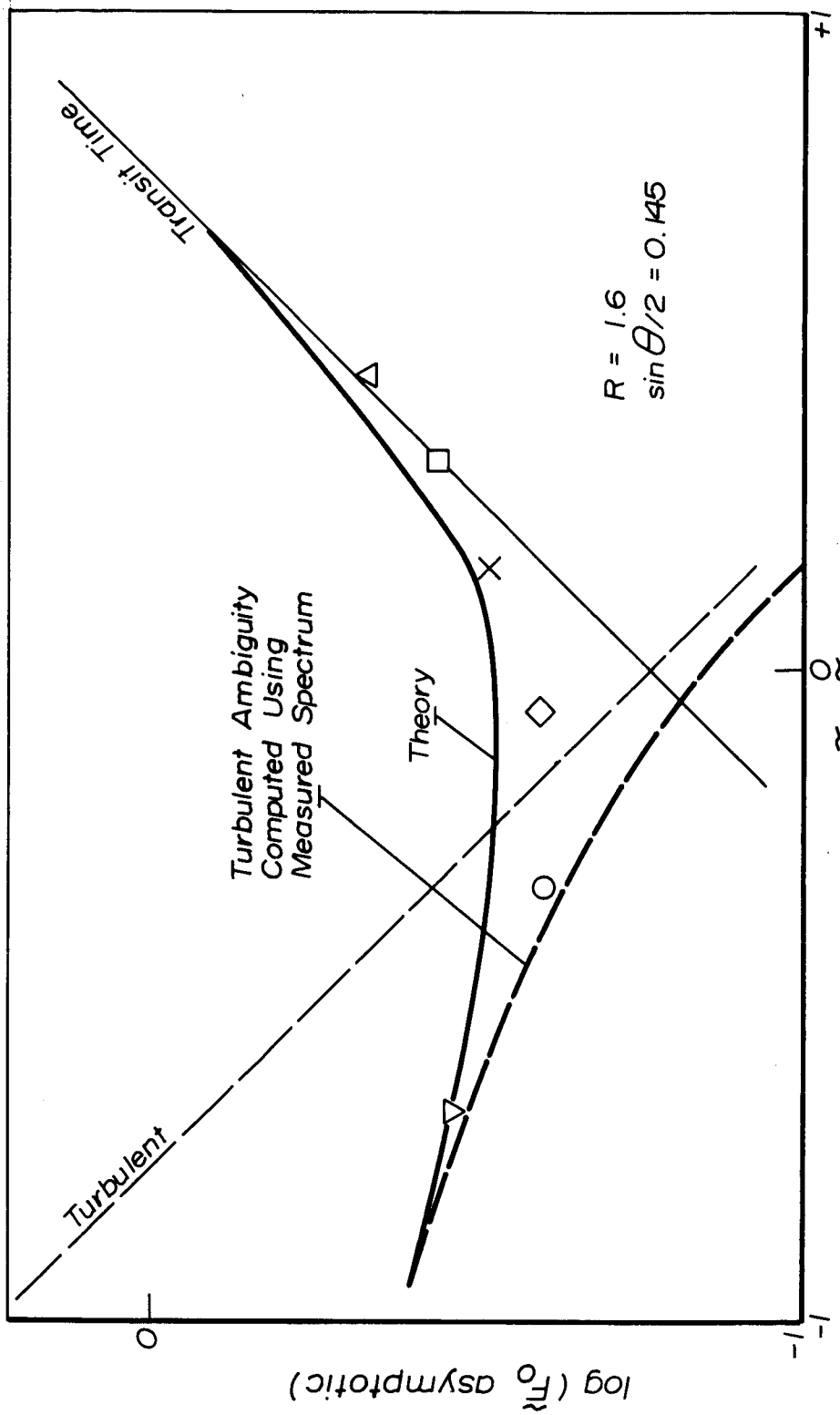

Figure 20: Comparison of Predicted and Measured Ambiguity Spectral Height in Turbulent Flow.

The measured values lie within 15% of the theoretical curve, but as in the case of the laminar measurements, seem to lie consistently below it. The fact that this trend seems consistent indicates that the theoretical constant computed in Appendix 2 may be about 10% high. This would not be surprising in view of the approximations used in evaluating the spectral height.

6.4 *The Electronic Noise*

The effect of the electronic noise on the height of the ambiguity spectrum was measured by varying the signal-to-noise ratio β. This was accomplished by means of a polaroid filter in the scattering beam which could be rotated to provide the desired reduction in the signal-to-noise ratio. The asymptotic values of the spectral height at large signal-to-noise ratios were subtracted from the measured values; the ratio of the amount of increase of the ambiguity height to the asymptotic value is shown in Figure (21) as a function of $\beta/\sqrt{N}$ for two different values of $N = \Delta\omega_f/\Delta\omega$. When $\beta/\sqrt{N} > 2$, the measurements are seen to lie within 10% of the theoretical curve given in equation (4.25). The deviation at $\beta/\sqrt{N} < 2$ is not surprising since the theoretical assumptions are no longer satisfied.

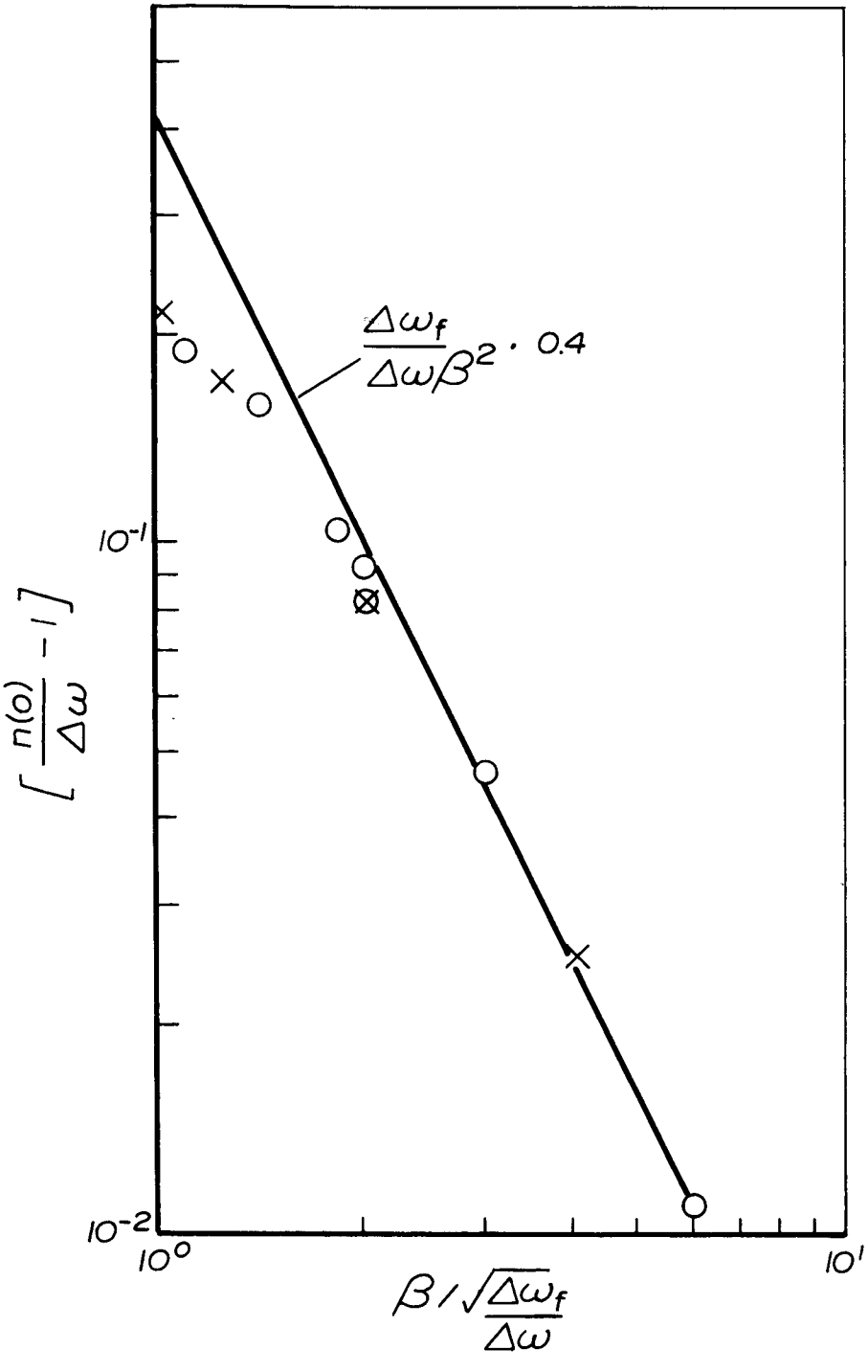

Figure 21: Comparison of Predicted and Measured Effect of the Electronic Noise.

6.5 Conclusions

The measurements taken in both laminar and turbulent flow agree with theory to within the experimental error. Trends in the data, nevertheless, seem to indicate that the theoretical prediction may be about 10% too high. However, since there are no adjustable constants in either theory or experiment, these results must be regarded as conclusive and the theory substantially correct.

7 SUMMARY AND CONCLUSIONS

7.1 Review of Results

The limitations on the use of a Laser-Doppler Velocimeter in the measurement of turbulence have been explored theoretically and experimentally.

The relationship between the size of the scattering volume and the resolution of the velocimeter was explored in Chapter 3 and criteria for accurate measurement were established; briefly, it was found that the turbulent fluctuations of wave number larger than the cutoff wave number associated with the largest dimension of the scattering volume were seriously attenuated.

The influence of the Doppler ambiguity on the measurement of spectra and other statistical quantities was examined and an exact theory for the spectrum of the random phase fluctuations was established. The Doppler ambiguity was seen to arise from the finite transit time of particles through the scattering volume, velocity fluctuations across the volume, and electronic noise, as well as velocity gradients and receiver aperture. The spectrum of the phase fluctuations was seen to be experimentally white

and proportional in height to the bandwidth of the Doppler ambiguity. Criteria for minimizing the height of the ambiguity spectrum were established and a critical scattering volume cutoff wave number for minimization was given as

$$\tilde{k}_{*crit} = 1.27\ (R \sin \theta/2)^{-1/2} \qquad (7.1)$$

where $R = 2\pi\bar{U}^2/\nu\bar{\omega}_o$ and where $\tilde{k}_*$ is the dimensionless cutoff wave number associated with that dimension of the scattering volume in the direction of the mean flow (see equation (3.5)).

7.2 *The Measurement of Spectra*

We must discuss the relationship between the resolution criteria and the criteria for minimizing the Doppler ambiguity.

For small scattering angles, the wave number associated with the largest dimension of the scattering volume, m_*, is related to k_* by

$$m_* = k_* \frac{\sin(\theta/2)}{\cos(\theta/2)} \qquad (7.2)$$

Using (7.1) we have

$$\tilde{m}_{*crit} = \tilde{k}_{*crit}\left[\frac{\sin(\theta/2)}{\cos(\theta/2)}\right] \simeq 1.27\left[\frac{(\sin\theta/2)}{R}\right]^{1/2} \quad (7.3)$$

We saw in Chapter 3 that $\tilde{m}_*$ determines the half power point of the spectral transfer function; that is, the wave number at which the measured spectrum is attenuated by 50%. Clearly $\tilde{m}_{*crit}$ determines the half-power point when the scattering volume is chosen for minimum Doppler ambiguity. Figure (22) shows a combined plot of, first, the wave number at which the turbulence to ambiguity ratio is unity and, second, the wave number of half power attenuation to which the spectrum may be corrected by subtracting the ambiguity (sin $\theta/2$ has been chosen as 0.145). By choosing values of $\tilde{k}_*$ greater than $\tilde{k}_{*crit}$ the half-power attenuation may be moved to as high a wave number as we please; however, the Doppler ambiguity will be sharply increased as will the error involved in obtaining the corrected spectral values.

To summarize the above comments into a practical plan for research: in all but the most unusual circumstances, the size of the scattering volume should be determined by (7.1) for

minimum ambiguity; the spectral values obtained should then be corrected by subtracting the Doppler ambiguity; and finally, the corrected values should be multiplied by the inverse transfer function $F_{11}(k_1)/F_o(k_1)$ to determine the true spectrum.

7.3 *Possible Alternatives for Spectral Measurement*

It has been suggested by some investigators that the Doppler ambiguity might be eliminated by using a frequency-tracking device. A frequency-tracker basically averages the product of the signal and a local oscillator, adjusting the local oscillator frequency to minimize the mean product. It is thus seen to be equivalent to a filter, operating on the input slewing rate, the filter characteristic being determined by the loop gain and the averaging characteristic. If the slewing rate of the phase fluctuations due to the Doppler ambiguity $\dot{\phi}$ were significantly different from the slewing rate of the turbulence ω_o, the averaging time of the frequency-tracker might be adjusted to average out the ambiguity fluctuations. Unfortunately, this attractive possibility does not correspond to reality; an examination of the spectra reveals that the slewing rates of the ambiguity and turbulence are quite similar

and thus indistinguishable on the basis of second order statistics. Clearly the frequency tracker can remove the Doppler ambiguity only by also removing some of the turbulence.

It was pointed out in Chapter 4 that two-point correlations may be performed by using two velocimeters since the Doppler ambiguity is uncorrelated if the scattering volumes do not overlap. If sufficient accuracy in determining the spectrum is not obtainable using the procedure suggested above, we may use two velocimeters whose scattering volumes are very close to each other - say within the turbulence microscale - although not overlapping; Figure (23) shows a possible configuration. After performing time correlations between the two outputs, we may obtain the spectrum by Fourier transforming the correlation. Since the Doppler ambiguity is uncorrelated between the two velocimeters and since the velocimeters are essentially sampling the same velocity fluctuation, the measured correlation is simply the correlation of the turbulence alone as is the resulting spectrum. Clearly, the spectrum can only be resolved to scales corresponding to the separation between the scattering volumes. This method of measuring spectra suffers from several obvious disadvantages: it requires two velocimeters instead of one, it requires very careful alignment to avoid overlapping and cross-talk, and considerable added effort is necessary to correlate and transform the outputs.

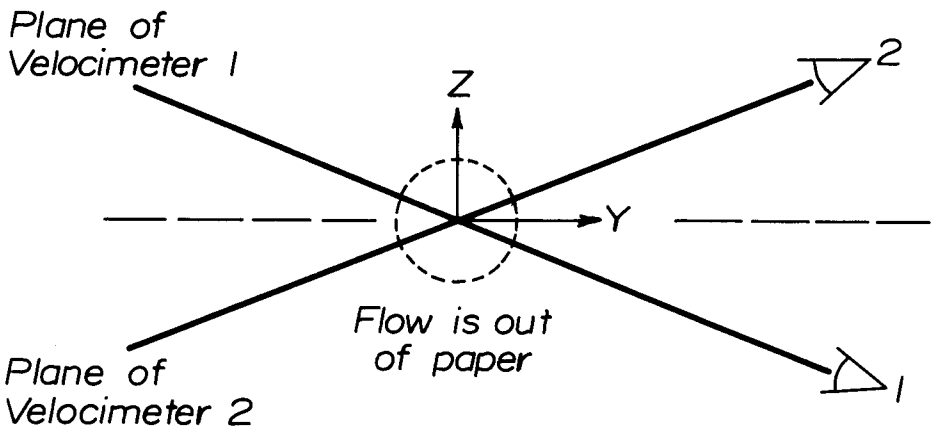

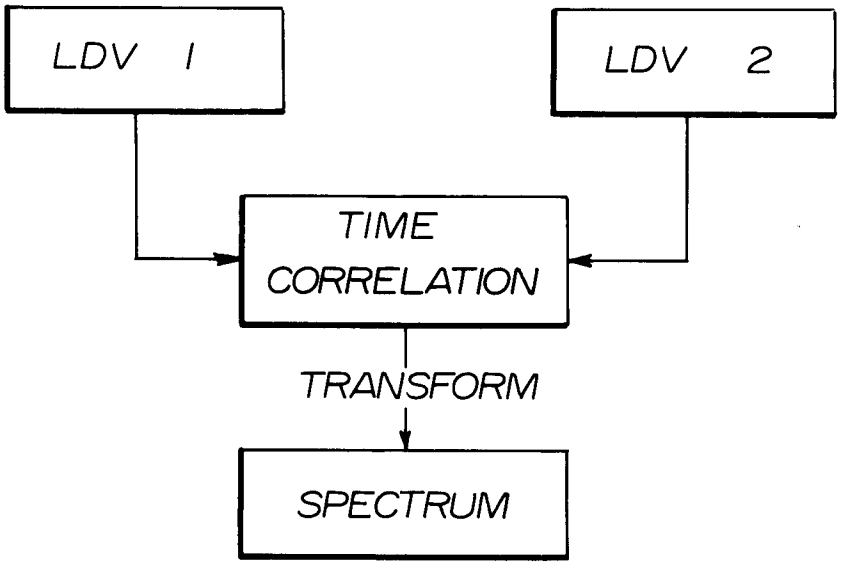

Figure 23: Setup for Measuring Spectra Using Two Velocimeters with Non-overlapping Scattering Volumes.

7.4 Conclusions

The influence of the Doppler ambiguity, together with the problems of resolution, have been shown to provide major limitations on the use of the Laser-Doppler Velocimeter in the measurement of turbulence.

It should be noted that these limitations apply to all Doppler Velocimeters regardless of the incident radiation. Table I shows an estimate of the dimensionless wave number at which the turbulence to ambiguity ratio is unity for a number of different applications. These estimates show that the possibility of measuring dissipation spectra in high speed or in geophysical flows using Doppler Velocimeters is quite remote.

Application	Radiation	λ	Velocity	ν_D	R	$\kappa\tilde{o}$
Grid Turbulence in Water	light	0.6 μ	1 m/s	500 kHz*	2	0.5
Grid Turbulence in Air	light	0.6 μ	1 m/s	500 kHz*	0.3	0.8
Wakes in Air	light	0.6 μ	300 m/s	150 MHz*	40	0.1
Clear Air Turbulence	radar	1 cm.	1 m/s**	100 Hz***	600	0.01
Oceanic Turbulence	sonar	.01 cm.	1 m/s**	20 kHz***	50	0.1

TABLE 1

*$\sin \theta/2 \sim 0.1$

**no mean velocity; $u' \sim 1$ m/s

***backscattering; $\sin \theta/2 \sim 1$

APPENDIX 1

A1 The Inverse Propagation Convolution*

We have from equation (2.9) that

$$i_{s_p}(t) = N \iint_S u_s(x,y_d,z,t)\, u_r^*(x,y_d,z)\,dxdz \qquad (A1.1)$$

If we define the two-dimensional Fourier transform over x and z, we may write

$$\tilde{u}_s(k,\ell,y_d,t) = \text{F.T.}\ \{u_s(x,y_d,z,t)\} \qquad (A1.2)$$

$$\tilde{u}_r(k,\ell,y_d) = \text{F.T.}\ \{u_r(x,y_d,z)\} \qquad (A1.3)$$

From Goodman we may write

* This analysis is a slightly revised form of Mayo (1970) and has been included here for completeness.

$$\tilde{H}(k,\ell,\Delta y) = e^{j(2\pi\Delta y/\lambda)}\ e^{-j[\lambda\Delta y(k^2+\ell^2)/4\pi]} \tag{A1.4}$$

as the transfer function for the Fresnel approximation of paraxial propagation over the distance Δy. Thus

$$\tilde{u}_r(k,\ell,y+\Delta y) = \tilde{u}_r(k,\ell,y)\ \tilde{H}(k,\ell,\Delta y) \tag{A1.5}$$

If we let

$$\begin{aligned} y &= y_p \\ \Delta y &= y_d - y_p \\ y + \Delta y &= y_d \end{aligned} \tag{A1.6}$$

we have

$$\tilde{u}_r(k,\ell,y_d) = \tilde{u}_r(k,\ell,y_p)\ \tilde{H}(k,\ell,y_d-y_p)$$

or

$$\tilde{u}_r(k,\ell,y_p) = \tilde{u}_r(k,\ell,y_d)\ \tilde{H}^{-1}(k,\ell,y_d-y_p) \qquad \text{(A1.7)}$$

Using (A1.4) it is clear that

$$\tilde{u}_r^{\,*}(k,\ell,y_p) = \tilde{u}_r^{\,*}(k,\ell,y_d)\ \tilde{H}(k,\ell,y_d-y_p) \qquad \text{(A1.8)}$$

Transforming back to space coordinates we have

$$u_r^{\,*}(x,y_p,z) = u_r^{\,*}(x,y_d,z) \circledast h(x,y_d-y_p,z) \qquad \text{(A1.9)}$$

where $\circledast$ defines a convolution over x and z and where

$$h(x,y,z) = \text{F.T.}^{-1}\{H(k,\ell,y)\} \qquad \text{(A1.10)}$$

$$= \left(\frac{e^{j2\pi y/\lambda}}{j\lambda y}\right)\ e^{j\pi(x^2+z^2)/\lambda y}$$

(A1.9) defines the inverse propagation convolution of $u_r(x,y_d,z)$ and may be written as

$$u_r^*(x_p,y_p,z_p) = \left[\frac{e^{j2\pi(y_d-y_p)/\lambda}}{j\lambda(y_d-y_p)} \right] \int_{-\infty}^{\infty}\int u_r^*(x,y_d,z) \cdot e^{j\pi[(x-x_p)^2 + (z-z_p)^2]/\lambda(y_d-y_p)}\, dxdz \qquad \text{(A1.11)}$$

But this is precisely the form of equation (2.11) and thus equation (2.12) is valid.

APPENDIX 2

A2 Evaluation of n(α), The Spectrum of the Phase Fluctuations

A2.1 Introduction

The goal of this section is to determine analytically the spectrum of the random phase fluctuations.

This analysis is essentially the same as that used by Lumley (1969) with minor changes resulting in an improved estimate of the spectral height. The analysis has also been extended to include the effects of turbulent broadening (see Chapter 3) and photodetection noise, as well as the random phase fluctuations introduced by the finite transit time of particles through the beam.

A2.2 The Doppler Signal

It was shown in Chapter (4) that the net signal from the scattering particles could be represented as

$$i(t) = F(t) \cos \omega_o t + G(t) \sin \omega_o t \qquad \text{(A2.1)}$$

where

$$F(t)=I\int_{\underset{\sim}{x}} e^{-\{[(x_o+ut)^2/2\sigma_1^2]+(y_o^2/2\sigma_2^2)+(z_o^2/2\sigma_3^2)\}}\cos[\omega\, t+\gamma(x_o)]d\xi(\underset{\sim}{x}_o) \tag{A2.2}$$

$$G(t)=-I\int_{\underset{\sim}{x}} e^{-\{[(x_o+ut)^2/2\sigma_1^2]+(y_o^2/2\sigma_2^2)+(z_o^2/2\sigma_3^2)\}}\sin[\omega\, t+\gamma(x_o)]d\xi(\underset{\sim}{x}_o) \tag{A2.3}$$

$$\overline{d\xi(\underset{\sim}{x}_o)d\xi(\underset{\sim}{x}_o')} = \begin{cases} 0, & \underset{\sim}{x}_o \neq \underset{\sim}{x}_o' \\ d\underset{\sim}{x}_o, & \underset{\sim}{x}_o = \underset{\sim}{x}_o' \end{cases} \tag{A2.4}$$

and where ω_o represents the instantaneous spatially averaged Doppler beat frequency while ω represents the local deviations from ω_o within the scattering volume.

If we assume the turbulence to be frozen in time as it is swept through the scattering volume, since $d\xi(\underset{\sim}{x}_o)$ is statistically independent at different times, F and G are identically distributed Gaussian random variables. Their correlation is given by

$$\overline{F(t)F(t')}=I^2\int_{\omega}\int_{\underset{\sim}{x}}\iiint e^{-\{(x^2/\sigma_1^2)+(y^2/\sigma_2^2)+(z^2/\sigma_3^2)\}}e^{-\{\bar{U}\tau(2x+\bar{U}\tau)/2\sigma_1^2\}} \tag{A2.5}$$

$$\cdot\ \cos[\omega\tau+\gamma(x)]\cos[\gamma(x)]dxdydzP(\omega)d\omega$$

where $\tau = t' - t$; a similar expression exists for $\overline{G(t)G(t')}$.

If the probability density of the turbulence is very nearly Gaussian with variance $(\Delta\omega_T)^2$ which was computed in Chapter (3), we take

$$P(\omega) = (1/\sqrt{2\pi}\ \Delta\omega_T)\ e^{-\omega^2/2(\Delta\omega_T)^2} \tag{A2.6}$$

Substituting (A2.6) into (A2.5) and neglecting terms of order $(\Delta\omega/\overline{\omega}_o)^2$ since the bandwidth is assumed small, we have

$$\begin{aligned} \rho_D(\tau) &= \overline{FF'}/\overline{F}^2 = \overline{GG'}/\overline{G}^2 \\ &\simeq e^{-(\Delta\omega)^2\tau^2/2} \end{aligned} \tag{A2.7}$$

where

$$\begin{aligned} (\Delta\omega)^2 &= (\Delta\omega_L)^2 + (\Delta\omega_T)^2 \\ \Delta\omega_L &= k_*\overline{U} = \sqrt{2}\ \overline{U}/\sigma_1 \end{aligned} \tag{A2.8}$$

As explained in Chapter (4), $\Delta\omega_L$ is the bandwidth introduced by the finite transit time of particles through the beam.

A2.3 *The Effect of Electronic Noise*

In addition to the Doppler signal, electronic noise arising from the detection process may also be present. To enhance the signal-to-noise ratio the Doppler signal and noise are usually passed through a band-pass filter.

It is shown in Appendix (3) that the noise may be represented by**

$$f(t)\cos\omega_o t + g(t)\sin\omega_o t \qquad \text{(A2.9)}$$

f and g are identically distributed Gaussian random variables; if we take the filter shape to be Gaussian for convenience, the correlation is given by

$$\rho_N(\tau) = \overline{ff'}/\overline{f^2} = \overline{gg'}/\overline{g^2} = e^{-(\Delta\omega_f\tau)^2/2} \qquad \text{(A2.10)}$$

where $\Delta\omega_f$ is the filter half-width and where it has been assumed

** This representation is well-known for the case where ω_o is fixed at the center frequency of the filter. Appendix (3) justifies the use of a fluctuating center frequency.

that $\overline{\omega_o'^2}/(\Delta\omega_f)^2 << 1$ (this must always be true if the turbulence is not to be seriously attenuated by the filter).

Hence the total electronic signal may be represented by

$$S(t) = (F + f)\cos\omega_o t + (G + g)\sin\omega_o t \qquad \text{(A2.11)}$$

Since F,G and f,g are statistically independent Gaussian variables, so are F+f and G+g with correlation

$$\rho(\tau) = \overline{(F+f)(F+f)'}/\overline{(F+f)^2} = \overline{(G+g)(G+g)'}/\overline{(G+g)^2}$$

$$\sigma_T^2\rho(\tau) = \sigma_D^2\rho_D(\tau) + \sigma_N^2\rho_N(\tau) \qquad \text{(A2.12)}$$

where σ_D^2 is the mean square Doppler signal, σ_N^2 is the mean square noise measured after the filter, and where

$$\sigma_T^2 = \sigma_D^2 + \sigma_N^2 \qquad \text{(A2.13)}$$

since the Doppler signal and noise are statistically independent and thus their variances are additive.

A2.4 *Instantaneous Velocity Measurements*

The total signal S(t) may be written as

$$S(t) = [(F+f)^2 + (G+g)^2]^{1/2} \cos(\omega_o t - \phi) \qquad (A2.14)$$

where

$$\phi = \tan^{-1}\{(G+g)/(F+f)\} \qquad (A2.15)$$

The usual sort of measuring circuit removes the amplitude information by amplifying and clipping, keeping only information on the zero crossings, and produces a signal proportional to frequency

$$\omega_1 = \omega_o - d\phi/dt \qquad (A2.16)$$

It was shown in Chapter (4) that since ω_o and $\dot{\phi}$ are uncorrelated, the spectrum of this signal is given by

$$(\overline{\omega}_o^2/\overline{U}^3)F_o(\alpha/\overline{U}) + \eta(\alpha) \qquad (A2.17)$$

where F_o is the spectrum of ω_o which is related to the turbulence

spectrum (see Chapter (3)) and $\eta(\alpha)$ is the spectrum of the phase fluctuations and is given by

$$\eta(\alpha) = (1/2\pi) \int_{-\infty}^{\infty} \overline{\dot{\phi}(t)\dot{\phi}(t+\tau)}\, e^{i\alpha\tau} d\tau \qquad \text{(A2.18)}$$

The value of $\eta(\alpha)$ at the origin is then

$$\eta(o) = (1/2\pi) \int_{-\infty}^{\infty} \overline{\ddot{\phi}\phi}\, d\tau = (1/2\pi)\overline{d\phi^2}/dt \qquad \text{(A2.19)}$$

If we let F+f and G+g represent the coordinates of a point in the x-y plane, the point moves in such a way that it has a circularly symmetric distribution since F+f and G+g are identically distributed Gaussian variables. ϕ is the angle subtended by the radius vector to the point and the x-axis. Since as time passes it becomes more and more likely that ϕ will have made one or more revolutions about the origin, ϕ is non-stationary and, therefore, $\eta(o)$ is non-zero.

The situation described here is a bit more complex than in Chapter (4) due to the introduction of the noise; nevertheless, the fact that F+f and G+g are identically distributed Gaussian

variables will permit an evaluation of $\eta(o)$ as well as yielding the shape of $\eta(\alpha)$.

From the geometrical representation of F+f and G+g and by differentiating (A2.15) we have

$$\dot{\phi} = v_\phi/r = rv_\phi/r^2$$

$$= \frac{(F+f)(\dot{G}+\dot{g}) - (G+g)(\dot{F}+\dot{f})}{(F+f)^2 + (G+g)^2} \qquad \text{(A2.20)}$$

where r is the radius vector to the point and v_ϕ is the azimuthal velocity. It is easy to show that v_ϕ and r are statistically independent. Since the distribution has circular symmetry, we may consider the joint distribution of v_ϕ and r where $\phi = 0$. Then $v_\phi = \dot{G} + \dot{g}$ and $r = F + f$ and they are independent. Thus

$$E\{\dot{\phi}(t)\dot{\phi}(t')\} = E\{\frac{V_\phi(t)\, V_\phi(t')}{r(t)r(t')}\}$$

$$= E\{\frac{1}{r}\frac{1}{r'}\}E\{v_\phi v_\phi'\} \qquad \text{(A2.21)}$$

where E{} will be used hereafter to denote the expected value; also

$$E\{rv_\phi r' v_\phi'\} = E\{rr'\}\, E\{v_\phi v_\phi'\} \tag{A2.22}$$

Hence

$$E\{\ddot{\phi}\phi'\} = \frac{E\{rv_\phi r' v_\phi'\}}{E\{rr'\}}\, E\{\frac{1}{r}\frac{1}{r}'\} \tag{A2.23}$$

For convenience we will define

$$\begin{aligned} a &= F + f \\ b &= G + g \end{aligned} \tag{A2.24}$$

Then using (A2.20)

$$E\{rv_\phi r' v_\phi'\} = E\{(\dot{a}b - b\dot{a})(\dot{a}b - b\dot{a})'\} \tag{A2.25}$$

Since a and b are Gaussian and statistically independent

$$E\{\dot{a}b\dot{a}'\dot{b}'\} = E\{aa'\}\,E\{\dot{b}\dot{b}'\}$$

$$= E\{aa'\}\,\partial^2/\partial t\partial t'\;E\{b(t)b(t')\} \qquad \text{(A2.26)}$$

$$= -\sigma^4\rho\;\partial^2\rho/\partial\tau^2$$

since $\tau = t' - t$, $\partial/\partial t = -\partial/\partial\tau$ and $\partial/\partial t' = \partial/\partial\tau$. Similarly

$$E\{\dot{a}b\dot{b}'a'\} = -\sigma^4(\partial\rho/\partial\tau)^2 \qquad \text{(A2.27)}$$

$$E\{b\dot{a}a'\dot{b}'\} = -\sigma^4(\partial\rho/\partial\tau)^2 \qquad \text{(A2.28)}$$

$$E\{b\dot{a}\dot{b}'a'\} = -\sigma^4\rho\,\partial^2\rho/\partial\tau^2 \qquad \text{(A2.29)}$$

Collecting and substituting into (A2.25), we have

$$E\{\dot{\phi}\dot{\phi}'\} = \frac{2\sigma^4(\rho'^2 - \rho\rho'')}{E\{rr'\}}\,E\{\frac{1}{r}\frac{1}{r'}\} \qquad \text{(A2.30)}$$

where $\rho' = \partial\rho/\partial\tau$, $\rho'' = \partial^2\rho/\partial\tau^2$. We need only find the joint

probability density for r and r' to evaluate (A2.30) in terms of known parameters.

A2.5 *Evaluation of* $\overline{\dot{\phi}^2}$

Since a and b are Gaussian and independent we may immediately write their joint distribution; that is*,

$$\text{Prob}\ \{c \leq a \leq c+dc,\ d \leq b \leq d+dd\} = (1/2\pi\sigma^2)\exp\{-(c^2+d^2)/2\sigma^2\}dcdd \tag{A2.31}$$

Transforming to polar coordinates and averaging over θ we obtain the probability distribution for r(t)

$$\text{Prob}\ \{z \leq r(t) \leq z + dz\} = (1/\sigma^2)e^{-z^2/2\sigma^2}zdz \tag{A2.32}$$

* We will drop the subscript T from σ_T and use σ^2 for the mean square Doppler signal plus noise since there is no danger of confusion with the beam diameter defined by (2.15).

It is straightforward to show that

$$E\{r^2\} = (1/\sigma^2) \int_0^\infty z^3 e^{-z^2/2\sigma^2} dz = 2\sigma^2 \qquad \text{(A2.33)}$$

However,

$$E\{ \frac{1}{r}\frac{1}{r} \} = (1/\sigma^2) \int_0^\infty z^{-1} e^{-z^2/2\sigma^2} dz = \infty \qquad \text{(A2.34)}$$

Hence from (A2.23), $\overline{\dot{\phi}^2} = \infty$ and thus $\overline{\dot{\phi}\dot{\phi}'}$ is singular at the origin. This behavior is not surprising: since v_ϕ and r are independent, the same values of v_ϕ may occur for small r as for large r; hence very large values of v_ϕ may occur when r is small.

Because of the singularity at the origin of $\overline{\dot{\phi}\dot{\phi}'}$, we may expect the spectrum of $\eta(\alpha)$ to be very broad - the behavior at infinity will depend on the type of singularity.

A2.6 *The Joint Probability Density for r and r'*

Since a and a' are jointly Gaussian with correlation ρ we may write

$$\text{Prob}\ \{c \leq a \leq c+dc,\ d \leq a' \leq d+dd\}$$

$$= (1/2\pi\sigma^2\sqrt{1-\rho^2})\exp\{-(c^2-2cd\rho+d^2)/2\sigma^2(1-\rho^2)\}dcdd \tag{A2.35}$$

The probability distribution for b and b' is identical to (A2.35) and since a and b are statistically independent, the joint probability distribution for a, a', b, b' is the product of the individual distributions; that is,

$$\text{Prob}\left\{\begin{matrix} c\leq a\leq c+dc, & d\leq a'\leq d+dd \\ e\leq b\leq e+de & f\leq b'\leq f+df \end{matrix}\right\}$$

$$= \text{Prob}\left\{\begin{matrix} c\leq a\leq c+dc \\ d\leq a'\leq d+dd \end{matrix}\right\} \cdot \text{Prob}\left\{\begin{matrix} e\leq b\leq e+de \\ f\leq b'\leq f+df \end{matrix}\right\} \tag{A2.36}$$

By making the following coordinate transformations

$$\begin{aligned} c^2 + e^2 &= r^2 & d^2 + f^2 &= r'^2 \\ c &= r\cos\theta & d &= r'\cos\psi \\ e &= r\sin\theta & f &= r'\sin\psi \end{aligned} \tag{A2.37}$$

and noting that

$$dcdddedf \rightarrow rr'drdr'd\theta d\psi$$

we obtain the joint probability density for r,r',θ,ψ as

$$P(r,r',\theta,\psi)=[1/4\pi^2\sigma^4(1-\rho^2)]\exp\{-[r^2+r'^2-2\rho rr'\cos(\theta-\psi)]/2\sigma^2(1-\rho^2)\} \quad (A2.38)$$

By letting $\alpha = \theta$, $\beta = \psi - \theta$ and integrating over α and β we obtain the joint probability density for r and r'

$$P(r,r')=[1/2\pi\sigma^4(1-\rho^2)]e^{-(r^2+r'^2)/2\sigma^2(1-\rho^2)}rr'\int_{-\infty}^{\infty}e^{(\rho rr'\cos\beta)/\sigma^2(1-\rho^2)}d\beta \quad (A2.39)$$

From Gray, this last integral may be immediately identified as $2\pi I_o[\rho rr'/\sigma^2(1-\rho^2)]$ where I_o is a modified Bessel function of the second kind. Hence

$$P(r,r')=[1/\sigma^4(1-\rho^2)]e^{-(r^2+r'^2)/2\sigma^2(1-\rho^2)}rr'I_o\{\rho rr'/\sigma^2(1-\rho^2)\} \quad (A2.40)$$

We are now in a position to evaluate $E\{rr'\}$ and $E\{\frac{1}{r}\frac{1}{r'}\}$.

A2.7 *Asymptotic Forms of $I_o(x)$*

Anticipating difficulty in evaluating integrals involving $I_o(x)$ we note the following asymptotic forms:

$$I_o(x) = 1; \quad x \to o \tag{A2.41}$$

$$I_o(x) = e^x/\sqrt{2\pi x}\ ; \ x \to \infty \tag{A2.42}$$

In our case $x = \rho rr'/\sigma^2(1-\rho^2)$; clearly $\rho \to o$ corresponds to $x \to o$ and $\rho \to 1$ corresponds to $x \to \infty$.

A2.8 *Evaluation of $E\{rr'\}$ and $E\{\frac{1}{r}\frac{1}{r'}\}$*

Using (A2.40) we have

$$E\{rr'\} = \int_o^\infty\int_o^\infty rr' P(r,r')drdr' \tag{A2.43}$$

$$= [1/\sigma^4(1-\rho^2)]\int_o^\infty\int_o^\infty (rr')^2 e^{-(r^2+r'^2)/2\sigma^2(1-\rho^2)} I_o\{\rho rr'/\sigma^2(1-\rho^2)\}drdr'$$

and

$$E\{\frac{1}{r}\frac{1}{r'}\} = \int_0^\infty\int_0^\infty \frac{1}{r}\frac{1}{r'} P(r,r')drdr' \tag{A2.44}$$

$$=[1/\sigma^4(1-\rho^2)]\int_0^\infty\int_0^\infty e^{-(r^2+r'^2)/2\sigma^2(1-\rho^2)} I_o\{\rho rr'/\sigma^2(1-\rho^2)\}drdr'$$

We shall evaluate this in two pieces - in the limits as $\rho \to 1$ and $\rho \to o$; then we shall use these asymptotic forms in the evaluation of $\eta(o)$.

Using the asymptotic forms of I_o in (A2.41) and (A2.42) it is straightforward to obtain

$$E\{rr'\}|\rho \to o = \sigma^2 \pi/2 \tag{A2.45}$$

$$E\{rr'\}|\rho \to 1 = 2\sigma^2\rho \tag{A2.46}$$

$$E\{\frac{1}{r}\frac{1}{r'}\}|\rho \to o = \pi/2\sigma^2 \tag{A2.47}$$

$E\{\frac{1}{r}\frac{1}{r'}\}|\rho \to 1$ is quite complicated, however, and is given by

$$(1/\sigma^2)\int_0^\infty (r'/\sigma)^{-\frac{1}{2}} e^{-r'^2/2\sigma^2} \{\int_0^\infty \frac{d(r/\sigma) e^{-(r-\rho r')^2/2\sigma^2(1-\rho^2)}}{[2\pi(1-\rho^2)(r'/\sigma)]^{\frac{1}{2}}}\} d(r'/\sigma)$$

(A2.48)

It is shown in Appendix (4) that the inner integral may be approximated by

$$0.862/\sqrt{1-\rho^2} \quad \text{when} \quad \rho r' < 1.35\sqrt{1-\rho^2}\cdot\sigma \qquad \text{(A2.49)}$$

$$\sqrt{\sigma}/\sqrt{\rho r'} \quad \text{when} \quad \rho r' > 1.35\sqrt{1-\rho^2}\cdot\sigma \qquad \text{(A2.50)}$$

Using (A2.49) and (A2.50) in (A2.48) we find

$$E\{\frac{1}{r}\frac{1}{r'}\}\Big|_{\rho\to 1} = (1/\sigma^2\rho)[2 + \tfrac{1}{2}\int_{\frac{0.91(1-\rho^2)}{\rho^2}}^\infty \frac{dt\, e^{-t}}{t}] \qquad \text{(A2.51)}$$

A2.9 *The Shape of the Spectrum*

It was previously concluded that since $\overline{\phi\phi'}$ was singular, the spectrum would be very broad - the shape depending on the type of singularity. From (A2.51) and from the small time expansion of ρ we have for $\sigma_D^2/\sigma_N^2 >> 1$

$$\int_{\frac{0.91(1-\rho^2)}{\rho^2}}^{\infty} \frac{dt\, e^{-t}}{t} \sim -\ln(\Delta\omega\tau) \qquad \text{(A2.52)}$$

Hence the singularity is logarithmic and the spectrum will fall off as inverse frequency. Since in the case of the Doppler signal without the noise the spectrum is determined only by $\Delta\omega$, we may expect the break to occur near $\alpha \sim \Delta\omega$. As was pointed out in Chapter 4, this is usually beyond the limit of the electronics and the spectrum is experimentally white with $\eta(\alpha) \simeq \eta(o)$ over the range of measurement.

A2.10 *Evaluation of $\eta(o)$*

From equations (A2.19) and (A2.30)

$$\eta(o) = (1/2\pi) \int_{-\infty}^{\infty} \frac{2\sigma^4 (\rho'^2 - \rho\rho'')}{E\{rr'\}} E\{\frac{1}{r}\frac{1}{r'}\}d\tau \qquad \text{(A2.53)}$$

From equation (A2.12)

$$2\sigma^4 (\rho'^2 - \rho\rho'') = 2\sigma_D^4 (\Delta\omega)^2 \rho_D^2 + 2\sigma_N^4 (\Delta\omega_f)^2 \rho_N^2$$

$$+ 2\sigma_N^2 \sigma_D^2 \{[(\Delta\omega)^2 + (\Delta\omega_f)^2] - \tau^2 [(\Delta\omega_f)^2 - (\Delta\omega)^2]^2\} \qquad \text{(A2.54)}$$

Substituting into (A2.53) and using the fact that the integrand of (A2.53) is an even function of τ we have

$$\eta(o) = (1/\pi)\int_o^\infty \frac{2\sigma_D^4 (\Delta\omega)^2 \rho_D^2}{E\{rr'\}} E\{\frac{1}{r}\frac{1}{r'},\}d\tau$$

$$+ (1/\pi)\int_o^\infty \frac{2\sigma_N^2 \sigma_D^2 \{[(\Delta\omega)^2 + (\Delta\omega_f)^2] - \tau^2 [(\Delta\omega_f)^2 - (\Delta\omega)^2]^2\}\rho_N\rho_D}{E\{rr'\}} E\{\frac{1}{r}\frac{1}{r'},\}d\tau$$

$$+ (1/\pi)\int_o^\infty \frac{2\sigma_N^4 (\Delta\omega_f)^2 \rho_N^2}{E\{rr'\}} E\{\frac{1}{r}\frac{1}{r'},\}\, d\tau$$

(A2.55)

The first term in equation (A2.55) is clearly the only term that would be present if there were no noise, while the last term is the only term that would be present if there were no Doppler ambiguity; the remaining term is then due to the interaction between the noise and the ambiguity. We shall call these $\eta_D(o)$, $\eta_I(o)$, $\eta_N(o)$ for Doppler ambiguity, interaction, and noise respectively; thus

$$\eta(o) = \eta_D(o) + \eta_I(o) + \eta_N(o) \qquad \text{(A2.56)}$$

If we are to now apply the asymptotic forms of $E\{rr'\}$ and $E\{\frac{1}{r}\frac{1}{r'}\}$, we must decide where to split the integral in τ. We shall always assume that the signal-to-noise ratio $\beta = \sigma_D/\sigma_N$ is greater than unity and that $\Delta\omega_f/\Delta\omega$, the ratio of the filter bandwidth to the Doppler bandwidth, is also much larger than unity. Under these assumptions, the large time behavior of ρ is dominated by ρ_D, hence $\Delta\omega$. By expanding ρ about $\tau = o$, it can be shown that as long as $(\Delta\omega_f/\Delta\omega\beta)^2 << 1$ the small time behavior of ρ is also dominated by $\Delta\omega$. Therefore, we will split the integrals at $\tau = 1/\Delta\omega$: when $\tau > 1/\Delta\omega$, we will use the $\rho \to 0$ form for $E\{rr'\}$ and $E\{\frac{1}{r}\frac{1}{r'}\}$; when $\tau < 1/\Delta\omega$, we will use the $\rho \to 1$ forms.

Since $\sigma^2 = \sigma_D^2 + \sigma_N^2$ and since we have previously assumed that $(\sigma_D/\sigma_N)^2 >> 1$, (A2.55) reveals that $\eta_I(o)$ will be of order σ_N^2/σ_D^2 while $\eta_N(o)$ will be of order σ_N^4/σ_D^4. Hence, we shall ignore the contribution of $\eta_N(o)$ and will consider only the interaction term $\eta_I(o)$.

$\eta_D(o)$ may now be written as

$$\eta_D(o) = (1/\pi) \int_{1/\Delta\omega}^{\infty} 2(\Delta\omega)^2 e^{-(\Delta\omega\tau)^2} d\tau$$

$$+ (1/\pi) \int_{o}^{1/\Delta\omega} (\Delta\omega)^2 e^{-(\Delta\omega\tau)^2} [2 + \tfrac{1}{2} \int_{\frac{0.91(1-\rho^2)}{\rho^2}}^{\infty} \frac{dte^{-t}}{t}] d\tau \qquad \text{(A2.56)}$$

If we take

$$\frac{0.91(1-\rho^2)}{\rho^2} \simeq (\Delta\omega\tau)^2 \qquad \text{(A2.57)}$$

it is straightforward to show that

$$\eta_D(o) \simeq (3.14/\pi)\ \Delta\omega \simeq \Delta\omega \qquad \text{(A2.58)}$$

Thus the height of the spectrum of the phase fluctuations due to the Doppler ambiguity alone is just equal to the Doppler bandwidth $\Delta\omega$.

From equation (A2.55) the contribution of the noise may be shown to be given by

$$(\Delta\omega_f\sigma_N^2/\pi\sigma_D^2)\{\int_o^N\{[1+(1/N^2)]-x^2[1-(1/N^2)]^2\}e^{-x^2[1-(1/N^2)]/2}$$

$$\cdot\ [2 + \tfrac{1}{2}\int_{\frac{0.91(1-\rho^2)}{\rho^2}}^{\infty}\frac{dte^{-t}}{t}]\ dx \qquad \text{(A2.59)}$$

$$+ 2\int_N^\infty\{[1+(1/N^2)]-x^2[1-(1/N^2)]^2\}e^{-x^2[1+(1/N^2)]/2}\ dx\}$$

where

$$N = \Delta\omega_f/\Delta\omega$$

and where N is assumed much greater than unity. It is not difficult to show that the second integral in (A2.59) goes to zero exponentially as N. The evaluation of the first integral is straightforward, although tedious; to second order in N

$$\eta_I(o) \simeq [0.40\ \Delta\omega_f/\beta^2]\{1 + (2/N^2)(\ell n N - 2.5)\} \qquad \text{(A2.60)}$$

where as before $\beta = \sigma_D/\sigma_N$.

Thus to first order in $\Delta\omega_f/\Delta\omega$ and σ_D/σ_N where we have assumed that $(\Delta\omega_f/\Delta\omega)^2 >> 1$, $(\sigma_D/\sigma_N)^2 >> 1$, and $(\sigma_N\Delta\omega_f/\sigma_D\Delta\omega)^2 << 1$; $\eta(o)$ is given by

$$\eta(o) = \Delta\omega\{1 + (0.4\ \Delta\omega_f/\Delta\omega\beta^2)\} \qquad \text{(A2.61)}$$

If β, the signal-to-noise ratio, is large enough, $\eta(o)$ reduces to

$$\eta(o) = \Delta\omega$$

which corresponds to the Doppler ambiguity alone.

APPENDIX 3

A3 Representation of the Photodetection Noise

It is well-known (c.f. Rice in Wax) that white noise passed through a bandpass filter may be represented by

$$f_1(t) \cos \omega_o t + g_1(t) \sin \omega_o t \tag{A3.1}$$

where ω_o is the center frequency of the filter and f_1, g_1 are identically distributed Gaussian random variables. If, for convenience, we take the filter to be of Gaussian shape with half-width $\Delta\omega_f$ then

$$\overline{f_1(t)f_1(t')}/\overline{f^2} = \overline{g_1(t)g_1(t')}/\overline{g^2} = e^{-(\Delta\omega_f \tau)^2/2} \tag{A3.2}$$

We saw in Chapter 4 that the Doppler signal could be represented as

$$F \cos \omega_o t + G \sin \omega_o t \qquad \text{(A3.3)}$$

where ω_o was the instantaneous volume averaged Doppler frequency and F,G were Gaussian random variables. Since the Doppler signal and the noise are statistically independent, it would be convenient to write the noise as

$$f \cos \omega_o t + g \sin \omega_o t \qquad \text{(A3.4)}$$

where f and g were identically distributed Gaussian random variables. Then we could write the signal plus noise as

$$(F + f) \cos \omega_o t + (G + g) \sin \omega_o t \qquad \text{(A3.5)}$$

where F+f and G+g would be identically distributed Gaussian variables.

From the definition of f_1, g_1 and the fact that in reality $\omega_o t$ is correctly written as

$$\overline{\omega_o} t + \Theta \quad \text{where} \quad \omega_o' = (d\Theta/dt) \tag{A3.6}$$

the f and g of (A3.4) must be given by

$$f = f_1 \cos \Theta - g_1 \sin \Theta \tag{A3.7}$$

$$g = g_1 \cos \Theta + f_1 \sin \Theta \tag{A3.8}$$

If the representation of (A3.4) is to be useful to us we must establish that the f,g defined by (A3.7) and (A3.8) are Gaussian. The correlations are easily seen to be given by

$$\begin{aligned} \overline{ff'} &= \overline{(f_1 \cos \Theta - g_1 \sin \Theta)(f_1' \cos \Theta' - g_1' \sin \Theta')} \\ &= \overline{f_1 f_1'} \ \overline{\cos (\Theta - \Theta')} = \overline{gg'} \end{aligned} \tag{A3.9}$$

and

$$\overline{fg'} = \overline{f_1 f_1'} \; \overline{\sin\ (\theta - \theta')} \tag{A3.10}$$

where $\theta - \theta'$ is given by

$$\theta(t) - \theta(t') = \int_{t'}^{t} \omega_o'(\tau)d\tau \tag{A3.11}$$

Clearly

$$\begin{aligned}
\overline{[\theta(t)-\theta(t')]^2} &= \iint_{t'}^{t} \omega_o'(\tau)\omega_o'(\tau')d\tau d\tau' \\
&= \overline{\omega_o'^2} \iint_{t'}^{t} \rho_o(\tau'-\tau)d\tau d\tau' \\
&= \overline{2\omega_o'^2}\, \tau \int_{o}^{\tau} [1-\frac{x}{\tau}]\rho_o(x)dx
\end{aligned} \tag{A3.12}$$

where $\tau = t - t'$ and where ρ_o is the time correlation of the fluctuating Doppler frequency. Since $\overline{[\theta-\theta']^2}$ depends only on time differences, $\theta - \theta'$ is stationary.

If the turbulent velocities are taken to be Gaussian*, we may compute

$$\overline{\cos(\theta-\theta')} = \int \cos(\theta-\theta')\, e^{-(\theta-\theta')^2/2\sigma^2}\, d(\theta-\theta') = \exp\{-\overline{\omega_o'^2}\,\tau \int_o^\tau (1-x/\tau)\rho(x)dx\} \tag{A3.13}$$

where $\sigma^2 = \overline{[\theta-\theta']^2}$. Similarly it may be shown that

$$\overline{\sin(\theta-\theta')} = 0 \tag{A3.14}$$

To prove that f,g are Gaussian, we need only show that the characteristic functions of f and g are Gaussian. First we consider f,g at a single time. Using the fact that θ, f_1, g_1 are statistically independent it is easy to show that

$$\overline{e^{ik(f_1 \sin\theta + g_1 \cos\theta)}} = e^{-k^2\overline{f^2}} \tag{A3.15}$$

Hence f and g are Gaussian at one time.

*Even if not, equation (A3.11) is asymptotically Gaussian with appropriate restrictions (c.f. Lumley (1970)).

Now we consider f and g at different times

$$\overline{e^{ikf+i\ell g'}} = e^{-\frac{1}{2}(k^2\overline{f_1^2}+\ell^2\overline{g_1^2})} \int e^{-k\ell\overline{f_1 f_1'}\cos(\Theta-\Theta')} P(\Theta-\Theta') d(\Theta-\Theta') \tag{A3.16}$$

where

$$P(\Theta-\Theta') = (1/\sqrt{2\pi}\ \sigma)\ e^{-(\Theta-\Theta')^2/2\sigma^2} \tag{A3.17}$$

and where we have already integrated over $\Theta+\Theta'$. If we let $x = \Theta-\Theta'/\sigma$, the integrand of (A3.16) may be written

$$\int e^{-k\ell\overline{f_1 f_1'}} \cos \sigma x \quad 1/\sqrt{2\pi} \quad e^{-x^2/2}\, dx \tag{A3.18}$$

From (A3.9) and (A3.2) it is clear that we need only concern ourselves with times of no larger order than $1/\Delta\omega_f$. Since the root mean square of ω_o' must of necessity be much less than $\Delta\omega_f$ if the fluctuations are not to be attenuated by the filter, the correlation ρ_o falls much more slowly than $\overline{f_1 f_1'}/\overline{f^2}$. Hence for $\tau \sim 1/\Delta\omega_f$

$$\sigma^2 = \overline{(\Theta-\Theta')^2} \sim \omega_o'^2/(\Delta\omega_f)^2 << 1 \qquad \text{(A3.19)}$$

Thus σ is small.

Expanding the integrand of (A3.18) in powers of σ and neglecting terms of higher order than the second, we have

$$e^{-k\ell\overline{f_1 f_1'}} \cos \sigma x \simeq 1 + k\ell\overline{f_1 f_1'}\,(\sigma x)^2/2 \qquad \text{(A3.20)}$$

Integrating term by term, it is easy to show that to second order, the integral of (A3.18) is

$$e^{-k\ell\overline{f_1 f_1'}}\ \overline{\cos(\Theta-\Theta')}$$

Hence

$$\overline{e^{ikf+\,i\ell g'}} = e^{-\frac{1}{2}(k^2\overline{f_1^2} + 2k\ell\overline{f_1 f_1'}\ \overline{\cos(\Theta-\Theta')} + \ell^2\overline{g_1^2}} \qquad \text{(A3.21)}$$

which was to be proven; thus f,g are Gaussian at two times.

In summary we have shown that the filtered white noise may be represented as

$$f(t) \cos \omega_o t + g(t) \sin \omega_o t \tag{A3.22}$$

where f,g are identically distributed Gaussian variables as long as $\overline{\omega_o'^2}/(\Delta\omega_f)^2 << 1$ and where ω_o is the fluctuating Doppler frequency. The correlation $\overline{ff'}/\overline{f^2}$ is given by

$$\rho_N(\tau) = \overline{ff'}/\overline{f^2} = \overline{gg'}/\overline{g^2}$$

$$= e^{-(\Delta\omega_f\tau)^2/2} \; e^{-\overline{\omega_o'^2}\tau \int_o^\tau [1-x/\tau]\, \rho_o(x)dx} \tag{A3.23}$$

$$\simeq e^{-(\Delta\omega_f\tau)^2/2}$$

This is the form used in Appendix 2.

APPENDIX 4

A4 *Evaluation of the Integral Occurring in* $E\{\frac{1}{r}\frac{1}{r'}\}$ *as* $\rho \to 1$

From equation (A2.38) the integral to be evaluated is of the form

$$I = \int_0^\infty \frac{dx}{\sqrt{r}} \frac{e^{-(r-x)^2/2\varepsilon^2}}{\sqrt{2\pi\,\varepsilon}} \tag{A4.1}$$

where we have $x = \rho r'$ and $\varepsilon^2 = 1 - \rho^2$. Clearly as $\rho \to 1$, $\varepsilon \to 0$.

For $x \neq 0$, the method of Laplace (Erdélyi) may be used to give

$$I \sim \frac{1}{\sqrt{x}} + \frac{3\,\varepsilon^2}{8\,x^{5/2}} \tag{A4.2}$$

This is valid as long as

$$\frac{3\,\varepsilon^2}{8\,x^2} \to 0 \quad \text{as} \quad \varepsilon \to 0 \tag{A4.3}$$

Another expansion may be obtained by writing $x/\varepsilon = \xi$, $r/\varepsilon = \eta$

$$I = \frac{1}{\sqrt{2\pi\varepsilon}} \int_0^\infty \frac{d\eta}{\eta} e^{-(\eta-\varepsilon)^2/2} = \frac{1}{\varepsilon^{1/2}} \left\{ \int_0^\infty \frac{d\eta}{\eta} \frac{e^{-\eta^2/2}}{\sqrt{2\pi}} + \xi \int_0^\infty d\eta \sqrt{\eta} \frac{e^{-\eta^2/2}}{\sqrt{2\pi}} + o(\xi^2) \right\}$$

(A4.4)

where from Janke and Emde

$$\int_0^\infty \frac{d\eta}{\sqrt{\eta}} \frac{e^{-\eta^2/2}}{\sqrt{2\pi}} = \frac{1}{2^{5/4}\sqrt{\pi}} \int_0^\infty t^{-3/4} e^{-t} dt = \frac{\pi\sqrt{2}}{2^{5/4}\sqrt{\pi}} \frac{3/4}{0.919} = 0.862$$

(A4.5)

and

$$\int_0^\infty d\eta \sqrt{\eta} \frac{e^{-\eta^2/2}}{\sqrt{2\pi}} = \frac{1}{2^{3/4}\sqrt{\pi}} \int_0^\infty e^{-t} t^{-1/4} dt = \frac{\pi\sqrt{2}}{2^{3/4}\sqrt{\pi}} \frac{/4}{0.906}$$

(A4.6)

This expansion is valid if

$$\frac{x}{\varepsilon} \to 0 \quad \text{as} \quad \varepsilon \to 0$$

It is not difficult to show that there is no region of overlap where both expansions are valid. We may only say that

$$I \sim 1/\sqrt{x}\,, \qquad \varepsilon/x \to 0 \tag{A4.7}$$

$$I \sim \frac{0.862}{\varepsilon^{1/2}}\,, \qquad x/\varepsilon \to 0 \tag{A4.8}$$

Values of I in between must be obtained from (A4.4) by exact calculation.

It is possible to show, however, from (A4.4) that the maximum value of I is probably no greater than 25% above (A4.8). Hence to no more than about 10% error, we will approximate the integral by extending (A4.7) and (A4.8) until they intersect; thus we take

$$I = 1/\sqrt{x}\,, \qquad x > 1.35 \tag{A4.9}$$

$$I = \frac{0.862}{\varepsilon^{1/2}}\,, \qquad x \leq 1.35 \tag{A4.10}$$

BIBLIOGRAPHY

1. Abramowitz, M. and I. A. Stegun (ed.)(1964) *Handbook of Mathematical Functions*, National Bureau of Standards, U.S. Government Printing Office, Washington, D.C.

2. Batchelor, G. K. (1960) *The Theory of Homogeneous Turbulence*, Cambridge University Press, Cambridge, England.

3. Clark, W. H. (1970) "*Measurement of Two-Point Velocity Correlations in a Pipe Flow Using Laser Velocimeters*," Ph.D. Thesis, Dept. of Aerospace Engineering, Univ. of Virginia, Charlottesville, Virginia.

4. Clayton, (1954)"*Emulsions and Their Technical Treatment*," Churchill, London, England.

5. Corrsin, S. and G. Compte-Bellot (1966)"*The Use of a Contraction to Improve the Isotropy of Grid-Generated Turbulence*," J. Fluid Mech., Vol. 25, Part 4, pp. 657-682.

6. Davis, D. T. (1968) "*Analysis of a Laser-Doppler Velocimeter,*" ISA Transactions, 7, 1, pp. 43-51.

7. Erdélyi, A. (1956) *Asymptotic Expansions*, Dover, N.Y., N.Y.

8. Fabula, A. G. (1966) "*An Experimental Study of Grid Turbulence in Dilute High Polymer Solutions,*" Ph.D. Thesis, Dept. of Aerospace Engineering, The Pennsylvania State University, University Park, June 1966.

9. Foreman, J. W., Lewis, R. D. and Thornton (1966) "*Laser-Doppler Velocimeter for Measurement of Localized Fluid Velocities in Liquids,*" Proc. IEEE, 424.

10. George, W. K. and J. L. Lumley (1970) "*Limitations on the Measurement of Turbulence Using a Laser-Doppler Velocimeter,*" Proc. Electro-Optical Conference, New York, New York.

11. Goldstein, R. J. and D. K. Kreid (1967) "*Turbulent Flow Measurements Utilizing the Doppler Shift of Scattered Laser Radiation,*" Physics of Fluids, Vol. 10, No. 6, 1349, (June 1967).

12. Goodman, J. W. (1968) *Introduction to Fourier Optics*, McGraw-Hill, New York.

13. Greated, C. A. (1969) "*Effect of Polymer Additives on Grid Turbulence*," Nature, Vol. 224, December 20, 1969, pp. 1196-7.

14. Huffaker, R. M., C. E. Fuller, and T. R. Lawrence (1965) "*Application of Laser-Doppler Velocity Instrumentation to the Measurement of Jet Turbulence*," International Automotive Engineering Congress, Detroit, Michigan, January 13-17, 1969.

15. Janke, E. and F. Emde (1945) *Tables of Functions*, Dover, N.Y., N.Y.

16. Little, C. G. (1969) "*Acoustic Methods for the Remote Probing of the Lower Atmosphere*," Proc. IEEE, Vol. 57, No. 4, April 1969, pp. 571-578.

17. Lhermitte, R. M., "*Turbulent Air Motion As Observed by Doppler Radar*," Proc. 13th RADAR Meteorology Conf., McGill Univ., Montreal, Canada, August 20-24, 1968.

18. Lumley, J. L. and H. A. Panofsky (1964) *"The Structure of Atmospheric Turbulence,"* Interscience, N.Y., N.Y.

19. Lumley, J. L., W. K. George and Y. Kobashi (1969) *"The Influence of Doppler Ambiguity and Noise on the Measurement of Turbulent Spectra Using a Laser-Doppler Velocimeter,"* Proceedings of the Symposium on the Measurement of Turbulence in Liquids, Univ. of Missouri at Rolla (Sept., 1969).

20. Lumley, J. L. (1970) *Stochastic Tools in Turbulence,* Academic Press, N.Y., N.Y.

21. Mayo, W. T. (1969) *"Laser-Doppler Flowmeter - A Spectral Analysis,"* Ph.D. Thesis, Dept. of Electrical Engineering, Georgia Institute of Technology, May 1969.

22. Mayo, W. T. (1970) *"Spatial Filtering Properties of the Reference Beam in an Optical Heterodyne Receiver,"* Applied Optics, Vol. 9, No. 5, May 1970, pp. 1159-1162.

23. Morton, J. B. (1970) Private Communication.

24. Pao, Y. H. (1965) "*Structure of Turbulent Velocity and Scalar Fields at Large Wavenumber*," Physics of Fluids, 8, 1063.

25. Pike, E. R., D. F. Jackson, P. J. Bourke, and D. I. Page (1968) "*Measurement of Turbulent Velocities from the Doppler Shift in Scattered Laser Light*," Presentation at Division of Fluid Dynamics, Am. Phys. Soc., Lehigh, November 1967.

26. Rolfe, E., J. K. Silke, S. Booth, K. Meister, and R. M. Young (1968) "*Laser-Doppler Velocity Instrument*," NASA CR-1199, December 1968.

27. Ross, M. (1967) *Laser Receivers*, John Wiley and Sons, N.Y., N.Y.

28. Wax, N. (ed.)(1954) *Noise and Stochastic Processes*, Dover, N.Y.

29. Welch, N. E. and W. J. Tomme (1967) "*Analysis of Turbulence from Data Obtained with a Laser-Doppler Velocimeter*," AIAA Paper No. 67-179.

30. Wiseman, W. J. (1969) "*On the Structure of High Frequency Turbulence in a Tidal Estuary*," Tech. Report 59, Chesapeake Bay Institute, The Johns Hopkins University, Nov. 1969.

31. Wyngaard, J. C. and J. L. Lumley (1967) "A *Sharp Cutoff Spectral Differentiator*," Journal of Scientific Instruments, Vol. 44, pp. 363-365.

32. Wyngaard, J. C. (1968) "*Measurement of Small-Scale Turbulence Structure with Hot Wires*," Journal of Scientific Instruments (Journal of Physics E), Series 2, Vol. 1.

33. Yeh, H. and H. Z. Cummins (1964) "*Localized Fluid Flow Measurements with He-Ne Laser Spectrometer*," Applied Physics Letters, *4*, 176.

34. Gray, A. and G. B. Mathews (1966) "A *Treatise on Bessel Functions*," Dover, New York.

VITA

William Kenneth George, Jr. was born in Camp Shelby, Mississippi on April 19, 1945. He graduated from Cambridge High School in Cambridge, Maryland in 1963. He received the Bachelor of Engineering Science Degree, with a major in Engineering Physics, from the Johns Hopkins University in 1967. After one year as a graduate student in the Department of Mechanics at the Johns Hopkins University, he accepted a position as Instructor in Aerospace Engineering at the Pennsylvania State University.

He has presented papers on the use of Laser-Doppler Velocimeters at the ORDHAC Conference (August 1970), the Electro-Optical Conference (September 1970), the ASCE Conference on Water Resources (January 1971), the Pittsburgh Symposium on Flow (May 1971), and he has also co-authored several technical articles on the subject.

He is an associate member of Sigma Xi and a member of the American Association of University Professors.

April 21, 1971

To: Professors Carlson, Corrsin, Palmer and Long

Gentlemen:

Mr. William K. George will present his Ph.D. dissertation at a seminar given on Thursday, May 6 in 112 Latrobe Hall at 10:00 A.M.

The formal talk will be given in 45 minutes. There will be a question period after which the committee will meet to decide on the acceptability of the dissertation.

Title: AN ANALYSIS OF THE LASER DOPPLER VELOCIMETER AND ITS APPLICATION TO THE MEASUREMENT OF TURBULENCE.

Sincerely yours,

W. H. Schwarz

William H. Schwarz
Professor of Mechanics

cc: Prof. R. Green
Prof. C. Truesdell

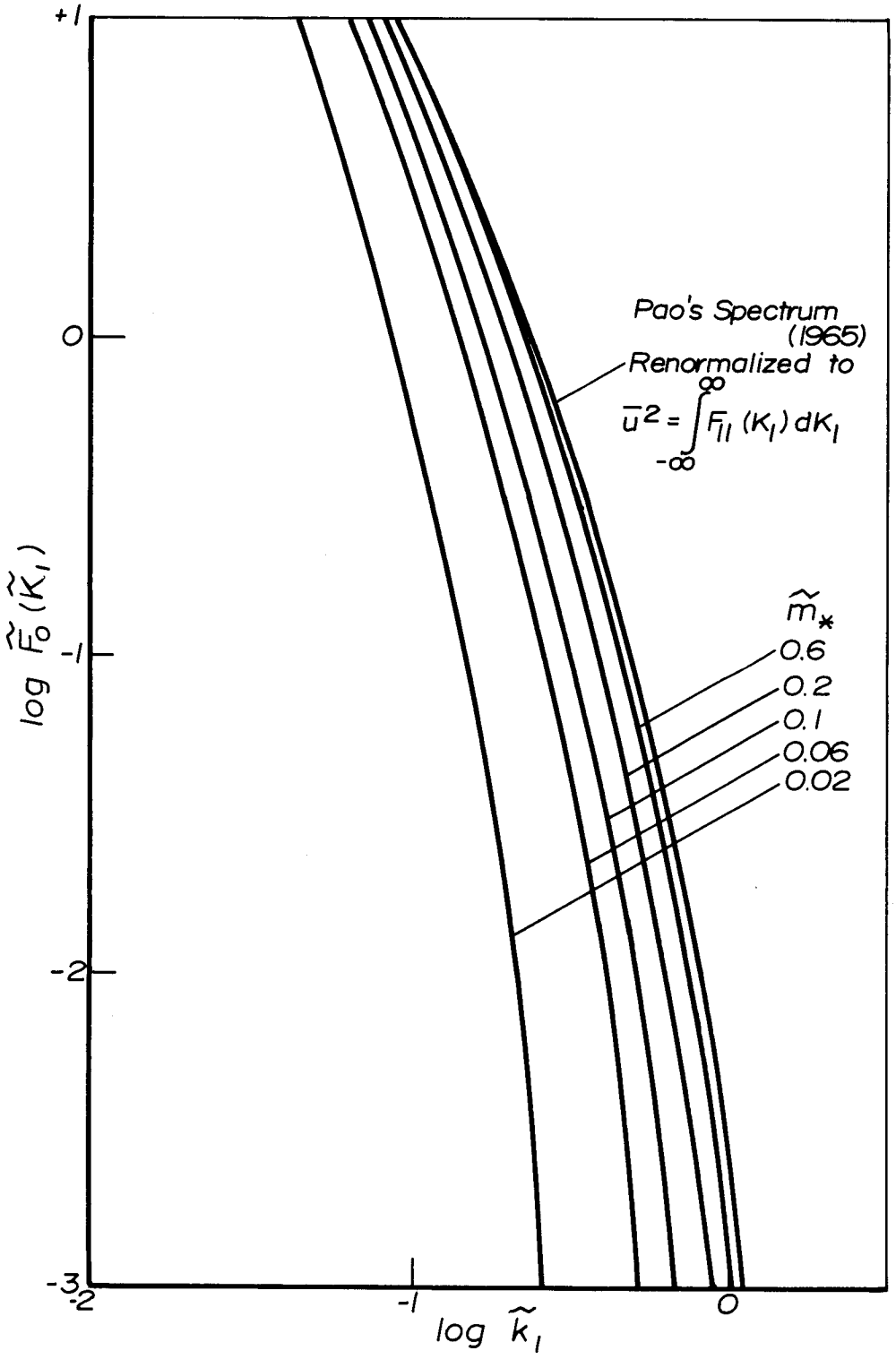

Figure 2: Measured Spectra Computed from Equation (3.13).

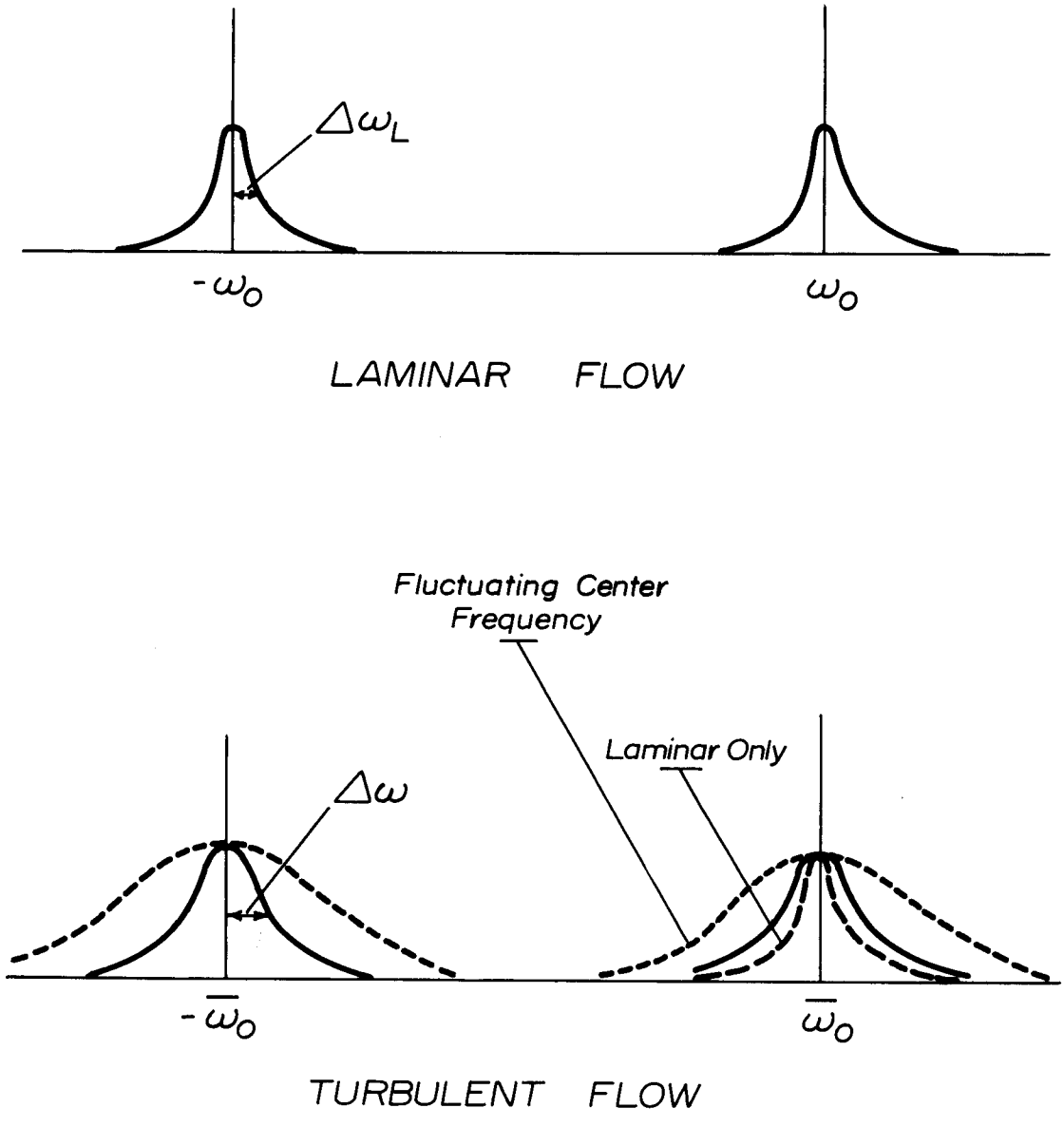

Figure 7: Spectrum of the Doppler Signal.

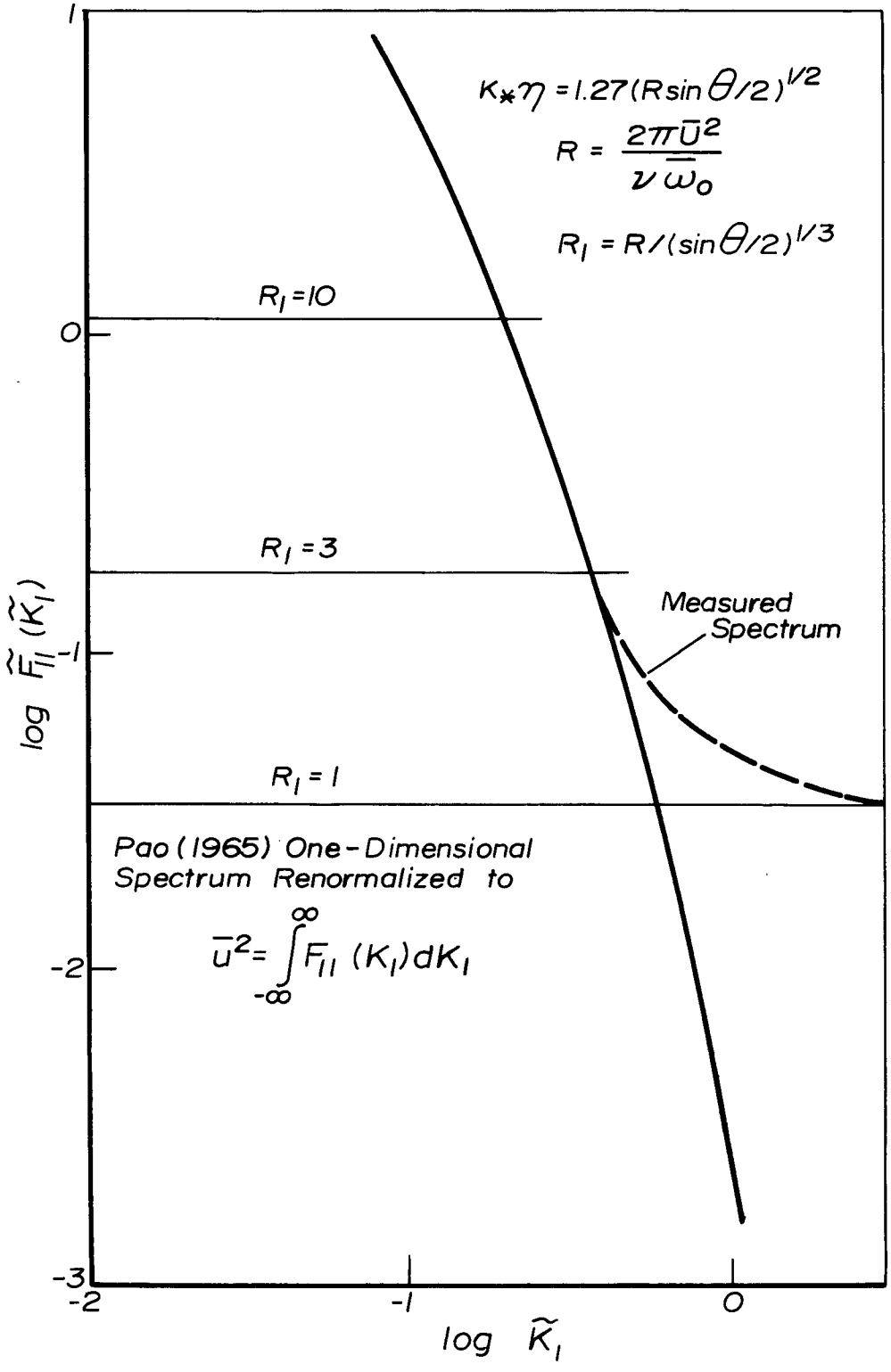

Figure 10: Optimum Ambiguity Spectra.

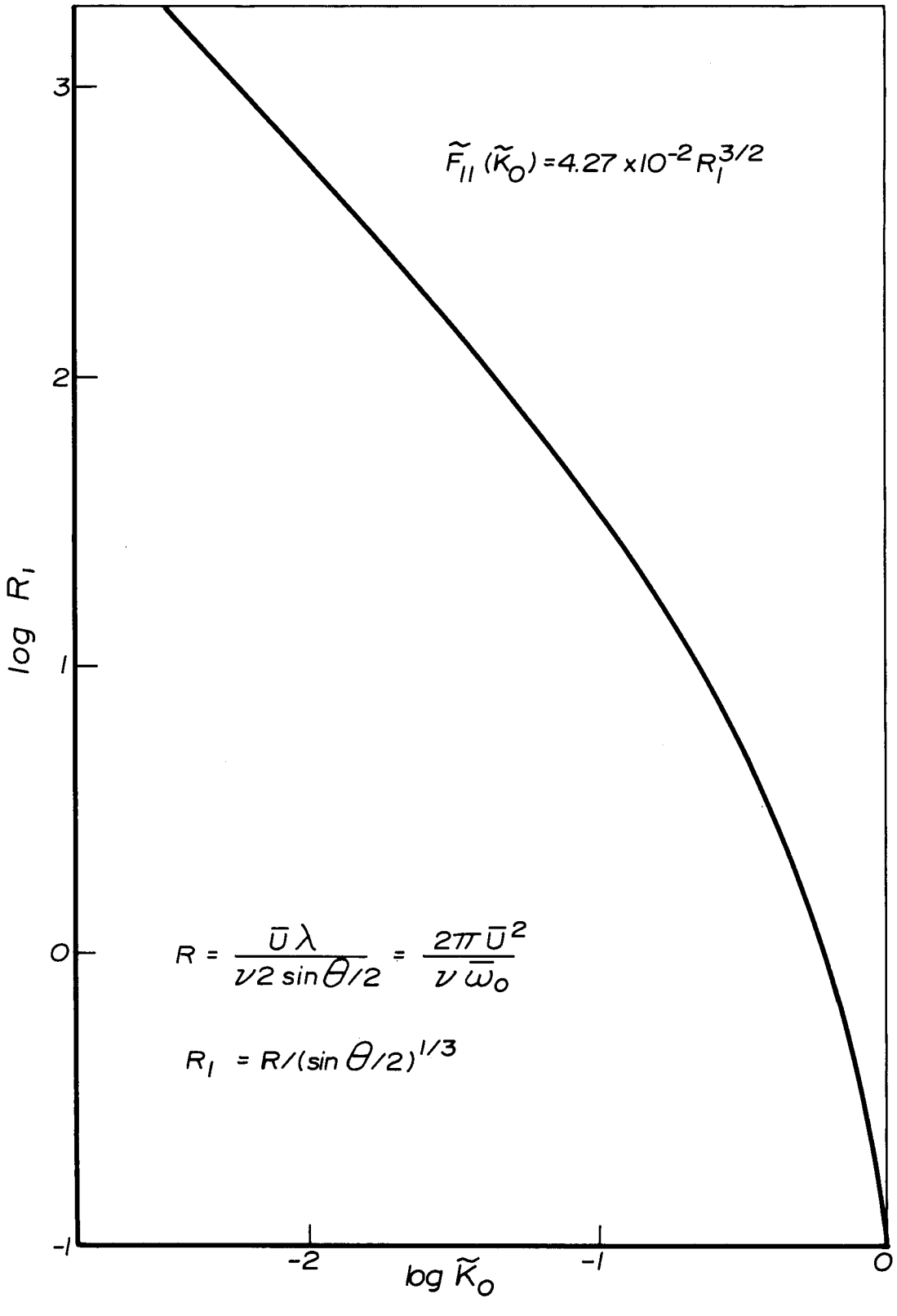

Figure 11: Value of $R_1 = 2\pi\bar{U}^2/\nu\bar{\omega}_o$ $(\sin \theta/2)^{1/3}$ for Unity Turbulence/Ambiguity at Indicated Wavenumber.

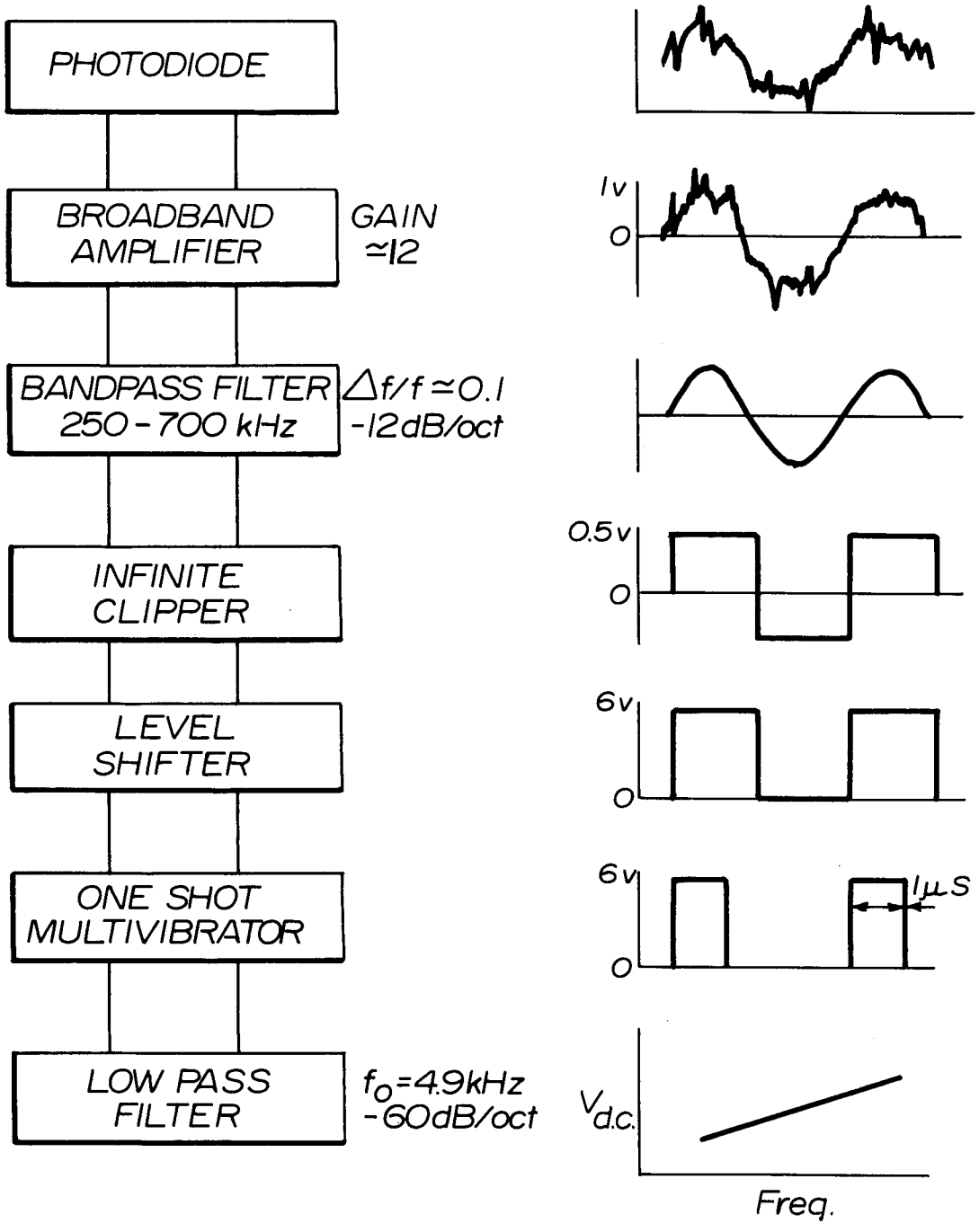

Figure 13: Frequency-to-Voltage Convertor

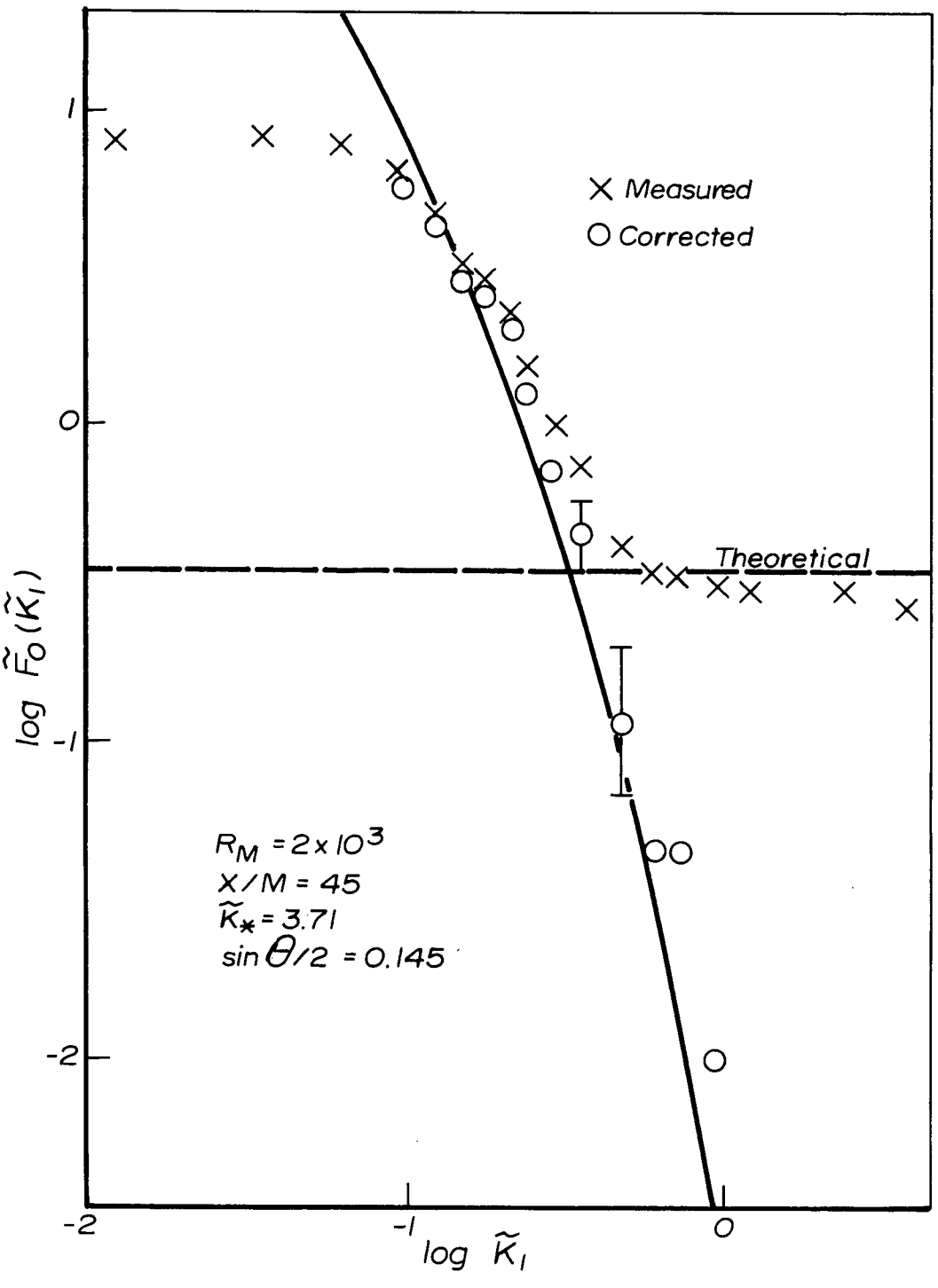

Figure 18: Comparison of Predicted and Measured Spectra in Turbulent Flow.

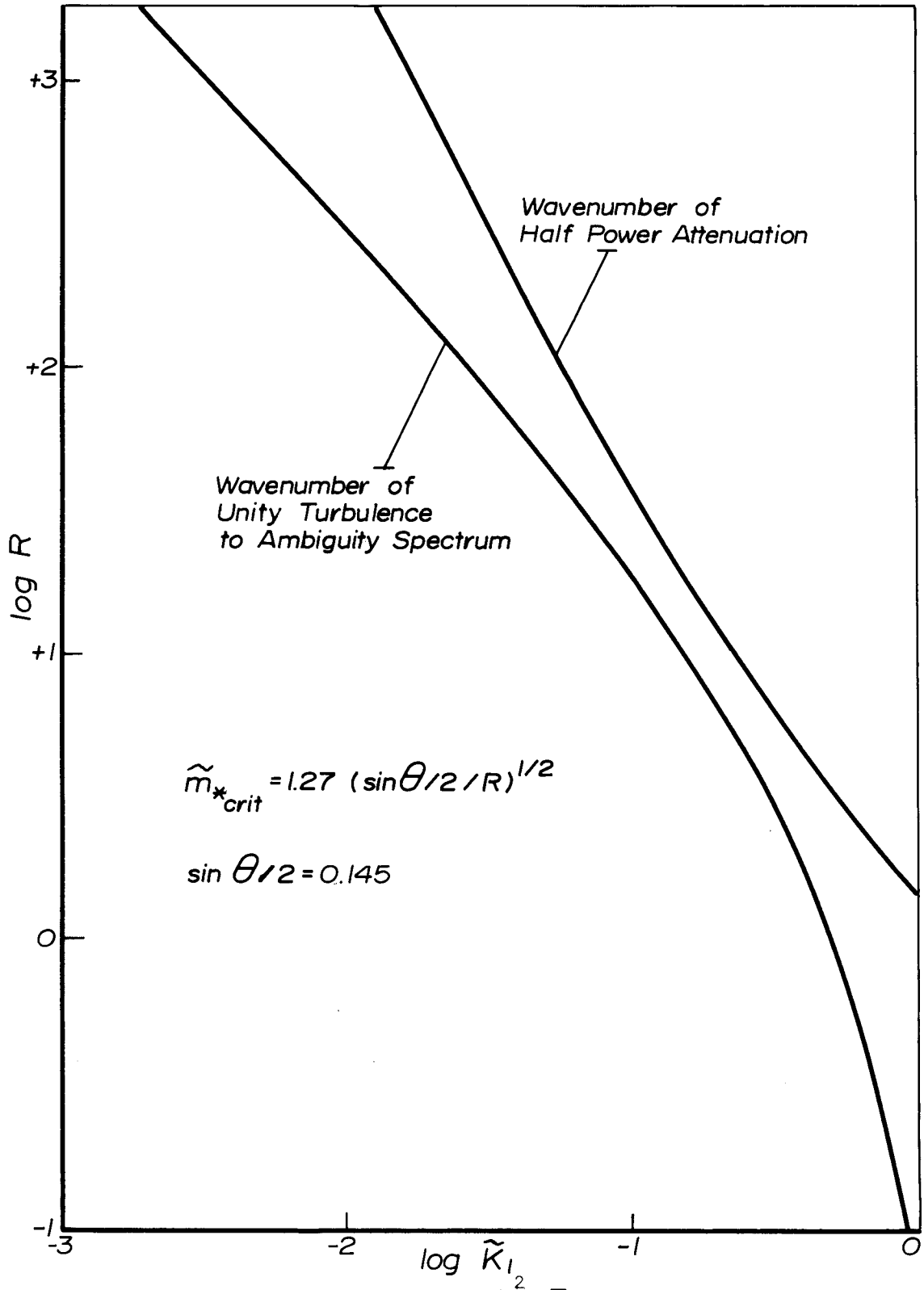

Figure 22: Combined Plot of $R = 2\pi\bar{U}^2/\nu\bar{\omega}_o$ for Unity Turbulence/ Ambiguity and Half Power Attenuation at Indicated Wavenumbers. Scattering Volume has been Selected for Optimum Ambiguity.